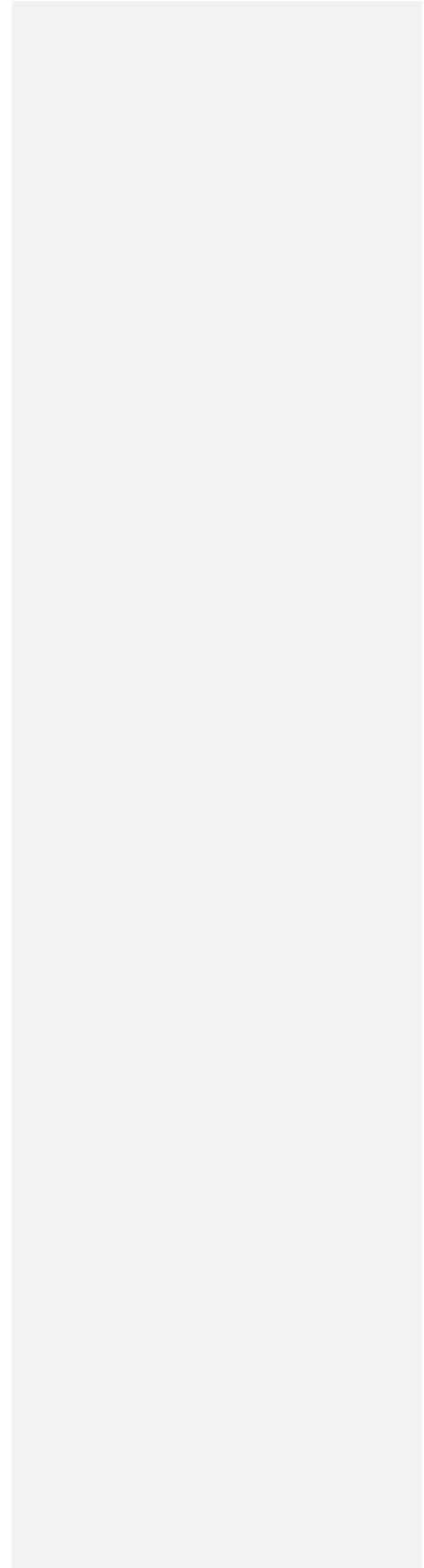**Buckling of U-Shaped Girders with Top-Flange Lateral Bracing**

by

Brian Scott Chen, B.S.C.E.

Thesis

Presented to the Faculty of the Graduate School of

The University of Texas at Austin

in Partial Fulfillment

of the Requirements

for the Degree of

Master of Science in Engineering

The University of Texas at Austin

May 1999

Buckling of U-Shaped Girders with Top-Flange Lateral Bracing
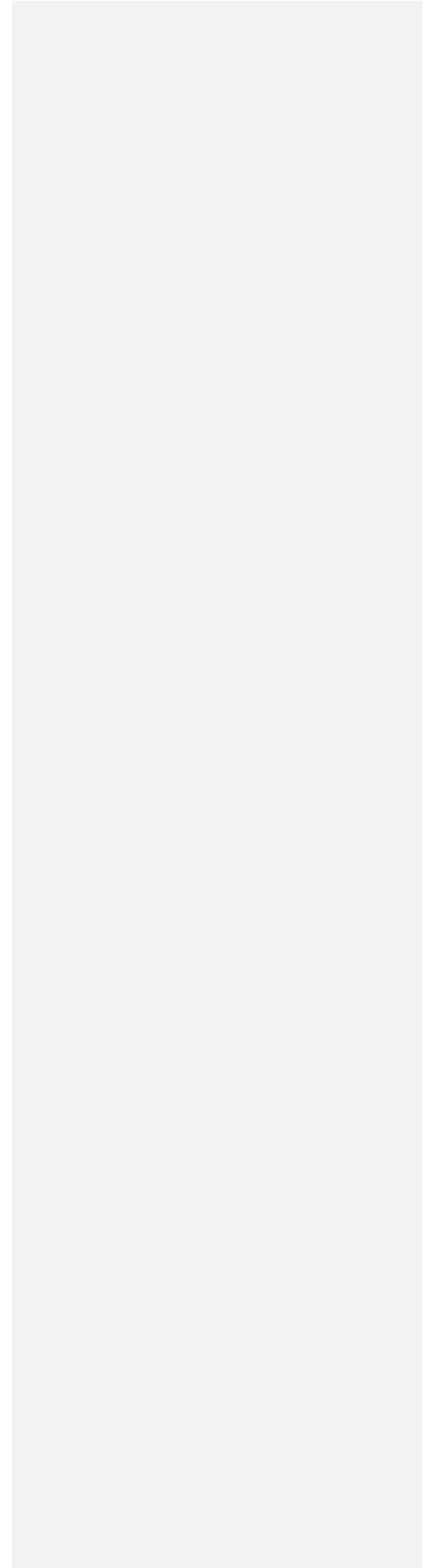
Approved by
Supervising Committee:

_____
Joseph A. Yura

_____
Karl H. Frank

To my father

ACKNOWLEDGEMENTS

ABSTRACT

Buckling of U-Shaped Girders with Top-Flange Lateral Bracing

Brian Scott Chen, M.S.E.

The University of Texas at Austin, 1999

Supervisor: Joseph A. Yura

Steel box girder systems are being used more frequently for curved bridges because of their torsional stiffness and aesthetic appearance. These systems typically consist of U-shaped girders placed side-by-side with a composite concrete deck acting as the top flange. A critical design stage for these girders occurs during casting of the bridge deck, when the non-composite steel section must support the entire construction load, including the wet concrete. During this period the top flanges are in compression and are susceptible to lateral-torsional buckling. Lateral bracing, typically in the form of a horizontal truss system, is installed to prevent the flanges from buckling and to increase the torsional stiffness of the girders. There is currently no existing codified design method for the lateral bracing of U-shaped girders. Because the bracing is not utilized once the concrete deck has cured, minimizing the amount of bracing will lead to more efficient designs.

In order to develop a design procedure, the behavior of U-shaped girders with top-flange lateral bracing was studied. A series of experimental tests were selected based on elastic finite element analyses. Variable parameters included brace stiffness, geometry, initial pretension force, and connection detail. Results included girder buckling loads, buckled shapes, and brace forces.

vi

TABLE OF CONTENTS

ix

LIST OF TABLES

x

LIST OF FIGURES

xii

xiii

NOTATION

DIMENSIONS AND SECTION PROPERTIES

b	Distance between girder webs (brace panel width)
s	Distance between adjacent brace points (brace panel length)
A_f	Area of one top flange
S_f	Section modulus for top flange about strong axis
S_g	Section modulus (top) for U-girder
Δ	Lateral deflection of top flange
Δ_o	Initial deflection of top flange
Δ_{lat}	Lateral deflection necessary to accommodate panel shortening
Δ_{sh}	Shortening of a brace panel due to girder bending
θ	Brace angle measured between diagonal brace and cross-strut

FORCES AND STRESSES

F_{br}	Diagonal brace force
F_{xs}	Cross-strut brace force
F_{yf}	Force necessary to cause yielding in both top flanges ($F_{yf} = 2A_f F_y$)
P, M	Experimentally applied ram load or moment
P_{cr}	Southwell predicted buckling load
P_e	Euler buckling load
P_{max}, M_{max}	Maximum experimentally applied ram load or moment

P_y, M_y	Ram load or moment causing first yield in top flanges using simple bending theory (calculation uses F_y)
σ_{max}	Maximum first and second-order compressive stress

MATERIAL PROPERTIES

F_{sy}	Static yield stress from tensile tests
F_y	Specified minimum yield stress

OTHER

β	Equivalent lateral stiffness of diagonal brace
β_{axial}	Axial stiffness of a tension brace member
$\beta_{coupler}$	Axial stiffness of coupler
β_i	Ideal brace stiffness

CHAPTER 1
Introduction

1.1 OVERVIEW

Trapezoidal box girder systems are being used more frequently for curved bridges because of their torsional stiffness and aesthetic appearance. A typical system consists of two U-shaped girders, usually called "tub" girders, placed side-by-side with a concrete slab connecting the top flanges as shown in Figure 1.1.

Cast-in-Place Concrete Slab

Stay-in-Place Metal Deck Forms

Steel U-Shaped Girders
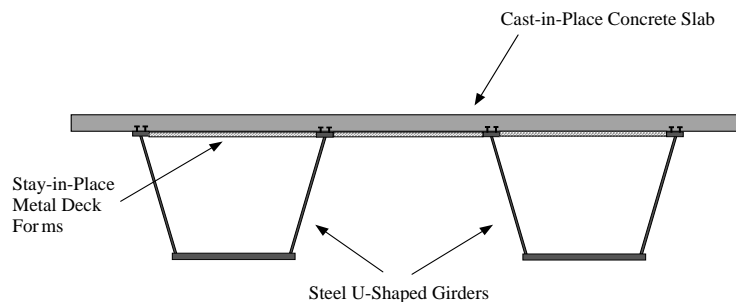
Figure 1.1 Cross-Section of a Box Girder Bridge System (Gilchrist, 1997)

Construction of box girder systems occurs in several stages. The steel U-shaped girders are first assembled in a fabrication shop by cutting the webs and flanges from plates and welding them together. The girders are typically fabricated in lengths of 12-35 m (40-120 ft.) so they can easily be transported to the construction site. Figure 1.2 shows a girder section prior to erection. At the job site, the segments are lifted into place and connected using bolted splice plates as seen in Figure 1.3. After the girders are bolted together, a stay-in-place metal

1

deck is placed across the top of the two girders. A concrete slab that will serve as the bridge deck is then poured into the metal deck forms in stages to control girder stresses and concrete shrinkage. When the concrete cures, shear studs previously placed on the top flanges allow the girder and deck to act compositely.

Figure 1.2 Cross–Section of U-Shaped Girder Segment (Gilchrist, 1997)
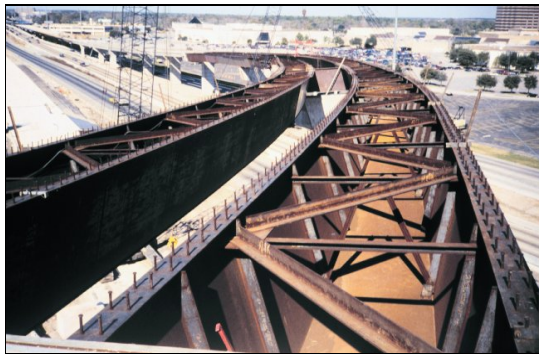
Figure 1.3 U-Shaped Girders During Erection (Gilchrist, 1997)

The composite action between the concrete deck and girders creates two closed trapezoidal boxes. The closed section characteristic provides a path for shear flow around the cross-section as shown in Figure 1.4, which dramatically increases the torsional rigidity. For comparison, closed cross-sections can often have torsional stiffnesses thousands of times greater than similar open sections (Basler, 1969).
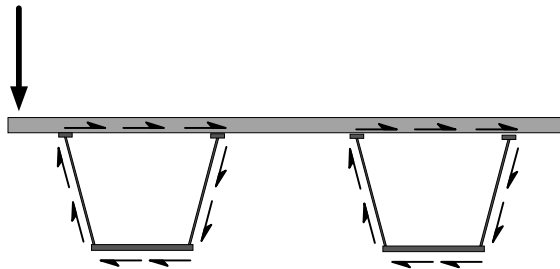
Figure 1.4 Shear Flow Resulting from Eccentric Load (Gilchrist, 1997)

1.2   NEED FOR U-GIRDER BRACING

The steel U-shaped girders feature narrow top flanges, especially in the positive bending moment regions of the bridge where the composite concrete deck is in compression. During the service life of the bridge, the neutral axis is located near the top flanges in the positive moment regions. Therefore, the width of the steel section's top flange is typically selected based only on the number of shear studs necessary to achieve composite behavior since larger flanges would provide little increase in the bending capacity. Prior to curing of the deck, the neutral axis of the steel girder is closer to the bottom flange. During this period

the top flanges are in compression and are susceptible to lateral-torsional buckling. Lateral bracing is necessary to prevent the flanges from buckling under loads encountered during fabrication, transport, erection, and deck placement. The bracing effectively closes the cross-section and enables the curved girders to resist the large torsional moments that occur when construction gravity loads are applied.

Once the concrete deck has cured, the bridge acts as a composite section. The deck provides continuous lateral bracing for the top flanges and also closes the cross-section of each U-girder. The hardened concrete deck provides the stability for the girder the internal bracing previously did. As a result, the lateral and torsional bracing placed in the U-girders for construction is no longer required after the concrete deck has hardened.

1.3   TYPES OF BRACING

There are two main types of bracing used in U-shaped girders. These braces can be classified as either a top lateral system or a diaphragm. Depending on the type used, the bracing can help increase a girder's torsional stiffness, reduce torsional distortion or warping of the cross-section, and/or prevent lateral buckling of the top flanges. In addition, these braces can also increase the bending strength of a U-shaped girder.

1.3.1   Top Lateral Systems

Top lateral bracing systems typically consist of a horizontal truss system placed near the top flanges along the entire length of the girder. The truss system can either be a single diagonal, as pictured in Figure 1.3, or an X-brace layout, as shown in Figure 1.1. Connecting the top flanges forms a pseudo-closed cross-section that increases the torsional stiffness of the girder significantly. The lateral

4

bracing also prevents the differential lateral movement of points along the top flanges that are connected by the bracing (points A and B in Figure 1.1).
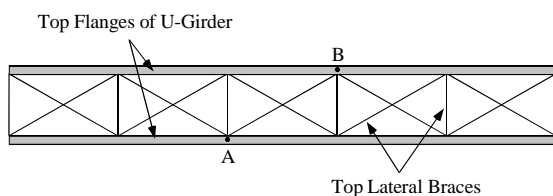
Figure 1.5 Top Lateral Bracing System

In theory, the bracing forces the top flanges to buckle between the brace points, which increases the bending capacity of the girder. Top-flange lateral bracing systems do not, however, prevent torsional distortion or warping of the cross-section, as shown in Figure 1.2. Warping occurs when noncircular cross-sections are subjected to torsion. In summary, a top lateral system can increase both the torsional stiffness and bending strength of a U-girder, but cannot prevent torsional distortion of the cross-section.
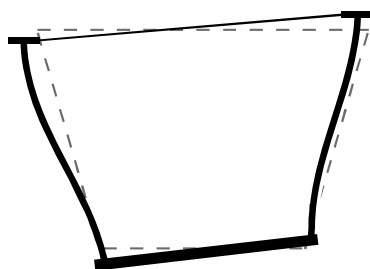
Figure 1.6 Torsional Distortion of Cross-Section

5

1.3.2 Diaphragms

Diaphragms are used to internally brace selected points along the length of a U-girder. Diaphragms are normally used to control distortion of the cross-section associated with torsional moments in a curved girder, but have also been shown to prevent lateral instability (Gilcrhist, 1997). Unlike top lateral systems, diaphragms do not affect the torsional stiffness of a U-girder.

Three common types of internal diaphragms, shown in Figure 1.1, are internal cross-frames, solid plates, and transverse stiffeners. Solid plates are placed at support points where piers apply concentrated forces to the girder and are used to prevent local crippling. K-shaped cross-frames are normally placed at regular intervals along the length of a girder. Transverse stiffeners, which are typically used to increase the shear strength of U-girder webs, are welded to the webs at locations of internal cross-frames. Stiffeners can also be used independently as diaphragms to help prevent distortion of the cross-section.
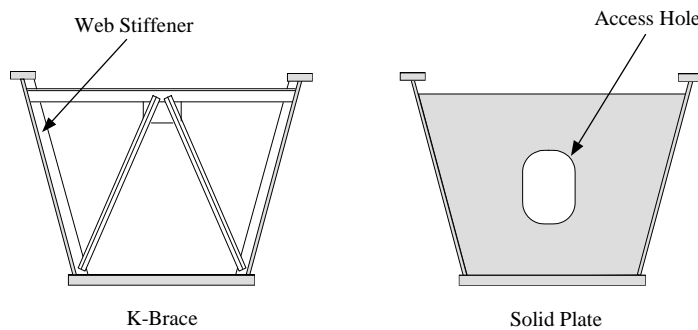
Figure 1.7 Interior U-Girder Diaphragms (Gilchrist, 1997)

6

In summary, diaphragms can increase the bending strength of a girder by controlling cross-section distortion, but cannot increase the torsional stiffness. Neither top-flange lateral bracing nor diaphragms alone are sufficient to adequately brace a curved U-girder.

1.4   CURRENT DESIGN CODE

The current AASHTO (American Association of State Highway and Transportation Officials) *Guide Specifications for Horizontally Curved Highway Bridges* provides very limited information on the lateral bracing requirements for the top flanges of steel box girders. Section 10.6 of the specification states:

> *These girders shall have diagonal top flange bracing to cause the steel section to act as a pseudo closed section. Diagonal top flange bracing shall be adequate to resist torsion applied to the steel section prior to the deck curing. Top flanges shall be assumed braced at points where interior bracing is located.*

To be an effective brace point, a lateral brace must have both adequate strength and stiffness (Winter, 1960). Currently, the AASHTO specifications provide no strength or stiffness requirements for lateral bracing of U-shaped girders. There is also no existing design method for lateral bracing of U-shaped girders.

1.5   OBJECTIVES OF RESEARCH

The work presented herein was part of research project 1395, "Trapezoidal Box Girder Systems", sponsored by the Texas Department of Transportation. The objective of this research project was to develop a reliable design approach for trapezoidal bridge systems.

7

The aim of this portion of the project was to determine the minimum bracing required to resist construction loads for U-shaped girders. The current specifications provide no means for determining the bracing necessary to resist torsional loading and prevent lateral-torsional buckling. It is important to minimize the bracing placed in U-shaped girders since this bracing is not utilized after the concrete deck of the box girder system has cured. Currently, the material and fabrication costs of the lateral bracing system make up a significant portion of the total box girder costs. For example, the top lateral bracing used in the bridge girder shown in Figure 1.3 increased the weight by nearly 12%. By reducing the amount of bracing currently being used for U-shaped girders, trapezoidal box girders can become a more efficient and cost effective bridge system.

In order to develop minimum bracing requirements, it was first necessary to understand the effect of the top-flange lateral bracing on the bending strength of U-shaped girders. An analytical study was conducted using elastic finite element modeling. Bifurcation loads and buckling modes obtained in the analysis were used to guide the selection of appropriate experimental test cases. Experimental tests were then conducted on a scale model of a rectangular U-shaped girder. Variable parameters included brace stiffness, geometry, initial pretension force, and connection detail. The scope of the investigation was limited to tension-only top-flange lateral bracing systems. Experimental test results provided girder buckling loads and buckled shapes to compare with the analytical results. Brace forces, which could not be obtained in the analytical program, were measured to compare with current design provisions.

CHAPTER 2

Analytical Program

2.1 GENERAL

An analytical program was undertaken to study the behavior of U-shaped girders with top-flange lateral bracing. A finite element model of an experimental test specimen was created to analyze the effects of variation in the number of brace points and brace stiffness. These results were used to select appropriate test cases for the experimental program.

2.2 GIRDER MODELING

The buckling behavior of a U-shaped girder can be understood by modeling the girder as two separate "half-girders" connected by a bottom flange. The wide bottom flange adds both torsional and lateral restraint to the half-girders. If either girder twists during buckling, the bottom flange must bend as illustrated in Figure 2.1. Therefore, the bottom flange restraint can be idealized as a torsional brace running continuously along the length of the girder. The stiffness of the continuous brace varies depending on whether the bottom flange bends in single or reverse curvature. Also, if the bottom of the girder is to move laterally, the bottom flange must bend about the weak axis of the girder. However, because the lateral moment of inertia of the bottom flange is so large the lateral restraint can be idealized on the half-girder as a continuous lateral support as shown in Figure 2.2.

The top-flange lateral bracing can be approximately modeled as discrete lateral springs. The stiffness of the lateral springs is based on the stiffness of the brace, the geometry of the brace layout, and whether the bracing is a tension-only

9

or tension-compression system. To obtain the buckling load for a complete U-girder, the buckling load of the half-girder is doubled.

$$\beta_b = \frac{M}{\theta} = \frac{2EI}{b} \qquad\qquad \beta_b = \frac{M}{\theta} = \frac{6EI}{b}$$
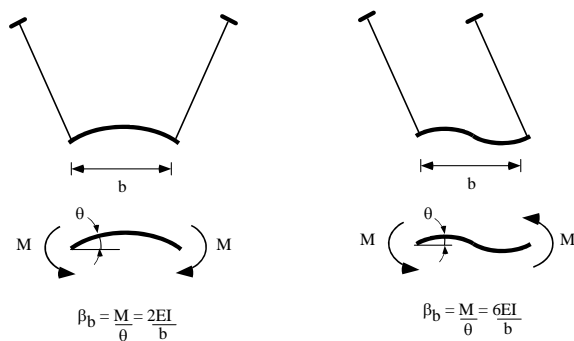
Figure 2.1 Torsional Restraint of Bottom Flange (Gilchrist, 1997)
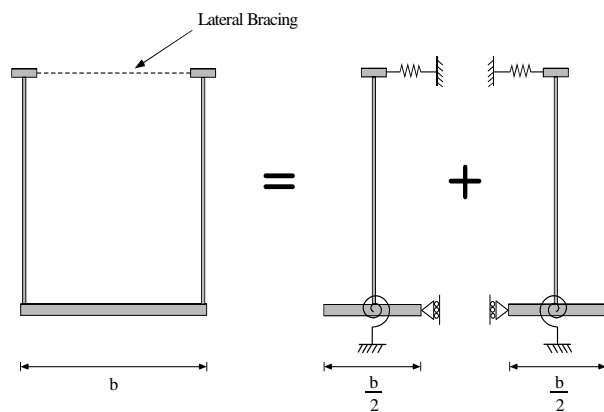
Figure 2.2 Half-Girder Model of a U-Girder with Top-Flange Lateral Bracing

10

2.3   BUCKLING BEHAVIOR OF U-GIRDERS

2.3.1   Column Analogy for Top-Flange Bracing

The bracing of the top flange of a U-Girder is similar to that of a column. Column bracing provides stability so that the column can support higher loads. The lateral bracing of a U-girder can similarly increase the buckling capacity by forcing the top flanges to buckle between brace points.

A relative brace controls the movement of adjacent stories or points along the length of a column or beam. Winter (1960) developed the dual parameters of strength and stiffness for bracing. In a relative column brace, the brace force is related to the initial column out-of-straightness, Δ_o, and the brace stiffness, β. The relative brace, shown as the spring at the top of the column in Figure 2.1, controls the movement at the top, Δ, relative to the column base. Summing moments about the base yields

$$P\Delta_T = \beta L \left(\Delta_T - \Delta_o \right) \tag{2.1}$$

where $\Delta_T = \Delta + \Delta_o$. For initially perfectly straight members where $\Delta_o = 0$, the brace force $F_{br} = \beta L$. The brace stiffness necessary to attain the buckling load between braces, P_o, is referred to as the ideal stiffness, β_i. In this case, $\beta_i = P_o/L$.

The relationship between P, β, and Δ_T is plotted in Figure 2.2. If $\beta = \beta_i$, the load can reach P_o only at very large displacement levels. Since $F_{br} = \beta L$, the resulting brace forces are also very high. If the brace stiffness is above ideal, P_o can be reached with much smaller deflections and brace forces. For example, if $\beta = 2\beta_i$, then $\Delta = \Delta_o$ at P_o. As the brace stiffness increases, the brace force decreases.

11
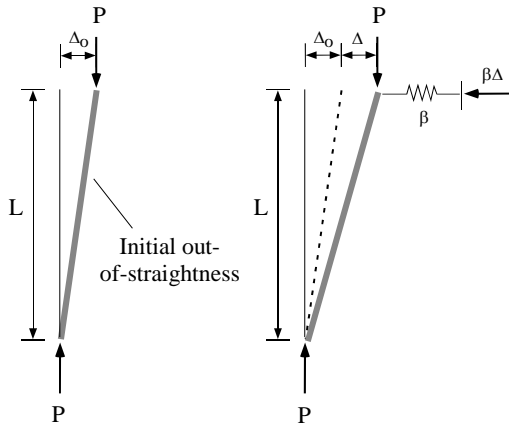
Figure 2.3 Relative Brace
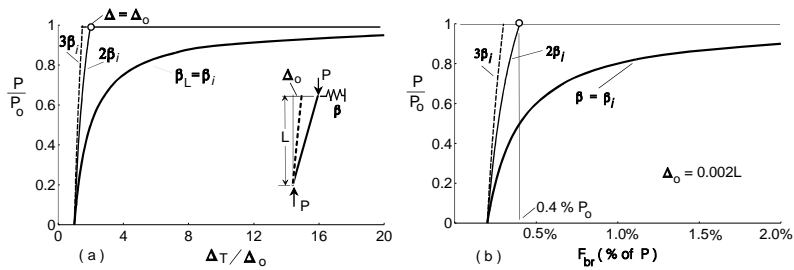
Figure 2.4 Effects of Increasing Brace Stiffness (Yura, 1993)

2.3.2   Description of BASP Computer Program

BASP, short for <u>B</u>uckling <u>A</u>nalysis of <u>S</u>tiffened <u>P</u>lates, is a two-dimensional elastic finite element program developed at the University of Texas at Austin (Akay, 1977; Choo, 1987). The program provides eigenvalue buckling modes for stiffened I-shaped beams and T-sections. It considers local and lateral-

12

torsional buckling including cross-section distortion. It will handle many types of restraints including lateral and torsional braces at any node point along the span as well as transverse and longitudinal stiffeners. BASP has been previously used to analyze braced beams. The solutions have been consistent with other finite element programs such as ABAQUS and are consistent with the works of others (Gilchrist, 1997; Yura, 1993).

A BASP model was created based on the half-girder analogy presented in Section 2.2. The model dimensions were based on the test specimen used in the experimental program. It consisted of a girder 12.19 m (40 ft.) in length, with pin supports located 1.83 m (6 ft.) from each end. Load was applied at each end of the girder, creating an 8.53 m (28 ft.) uniform moment region between supports, as shown in Figure 2.1. The cross-sectional dimensions are shown in Figure 2.2.

The boundary conditions for the model included lateral displacement restraints, rotational springs, and lateral springs and are shown in Figure 2.1. The continuous torsional restraint of the bottom flange was modeled as a series of discrete nodal springs. Their stiffnesses were calculated based on the dimensions of the bottom flange and the spacing of the nodes along the length of the girder. Lateral displacement was restrained at the load and support cross-sections due to the presence of internal stiffening frames in the U-girder. Top-flange lateral braces were modeled using lateral springs at various locations along the top flange.

Discrete and relative braces are two classifications for lateral beam braces. Relative braces control the relative lateral movement of two points along the length of a member. A truss system installed near the top flanges of a U-shaped girder is an example of a relative brace. Discrete braces, on the other hand, connect a point on the member to an independent point not on the member. Temporary guy cables are an example of a discrete brace. To achieve the same

13

performance, discrete braces require greater stiffnesses than relative braces (Yura, 1993).
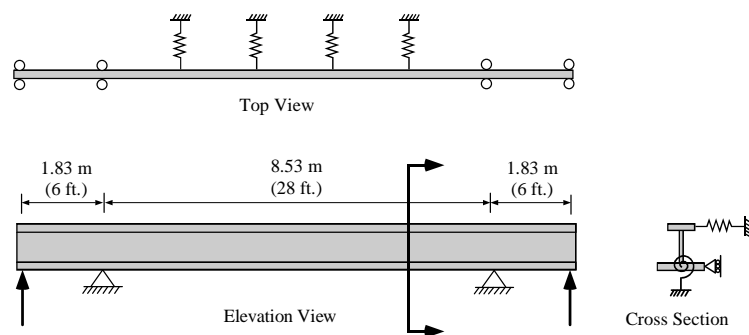
Figure 2.5 Boundary Conditions for BASP Model
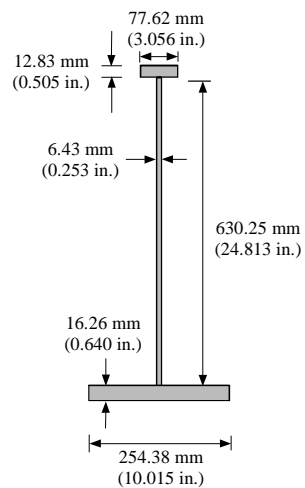
Figure 2.6 Cross-Sectional Dimensions of BASP Model

14

The top-flange lateral bracing system used in the experimental program was a relative bracing system. Because of the difficulties associated with modeling relative bracing on a single half-girder, discrete lateral springs were used to approximate the true relative bracing. The results, however, were used only for guidance in selecting appropriate experimental test cases.

2.3.3 Effect of Bottom-Flange Torsional Bracing

The wide bottom flange of the U-girder was modeled as a continuous torsional brace attached to the bottom flange of each half-girder. The stiffness of this brace was based on the width and thickness of the bottom flange as well as whether the bottom flange bent in single or reverse curvature during buckling.

Gilchrist (1997) studied the effects of bottom-flange torsional bracing on the buckling behavior of unstiffened half-girders. Figure 2.1 illustrates how increasing the torsional brace stiffness increases the buckling strength of the half-girder non-linearly. The buckling moment, M, is normalized by M_y, the moment necessary to cause yielding of the top flange of the half-girder using simple bending theory. The yield stress was taken to be 345 MPa (50 ksi), the minimum specified yield stress of the flanges of the test specimen used in the experimental program.

With no torsional bracing, the half-girder buckled into a single-wave between the supports at $M/M_y = 0.16$. A torsional brace of only 3.7 KN-m/rad/m (0.83 k-in/rad/in) was required to cause the girder to buckle into two-waves at $M/M_y = 0.22$. For a U-girder with a 254 mm (20 in.) wide bottom flange bending in single curvature, this corresponded to a bottom flange thickness of only 3.8 mm (0.15 in.). Increasing the brace stiffness beyond 200 KN-m/rad/m (45 k-in/rad/in) provided virtually no increase in buckling capacity. This was due to the effect of cross-section, which is illustrated in Figure 2.2. The introduction of torsional

15

bracing by the bottom flange of the U-shaped girder caused the first mode of buckling to be two-waves rather than the expected single-wave. This phenomenon was validated both in this experimental program as well as by Gilchrist (1997).
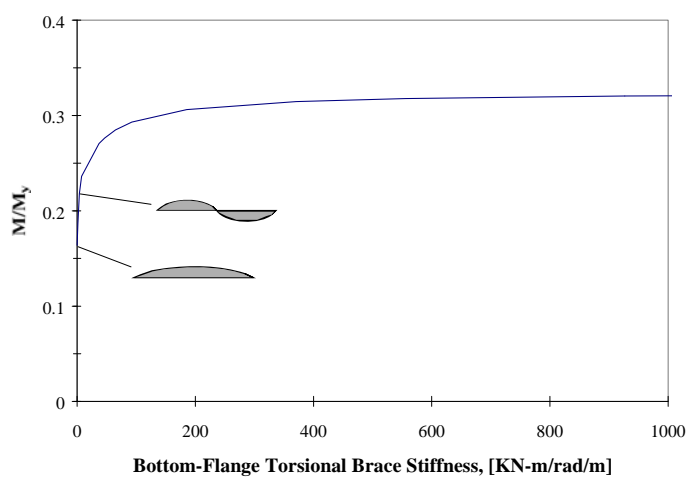
Figure 2.7 Effect of Increasing Bottom-Flange Torsional Brace Stiffness

Figure 2.8 Cross-Section Distortion (Gilchrist, 1997)

16

2.3.4 Effect of Cross-Section Distortion

Yura (1993) determined that even small amounts of web distortion have significant effects on the buckling load of torsionally braced beams. Gilchrist (1997) showed that by reducing web distortion with transverse stiffeners, the buckling capacity of the half-girder model could be increased substantially. Figure 2.1 shows that minimizing cross-section distortion allows higher buckling modes to be attained. By placing eight equally spaced 10 x 0.25 cm web stiffeners along the length of the half-girder, the buckling load reached was nearly twice that of the girder with the unstiffened web. This corresponded to a four-fold increase in buckling strength over the girder with no web stiffeners or bottom-flange torsional bracing. The third and fourth buckling modes were attained at torsional stiffnesses of 185.3 KN-m/rad/m (41.7 kip-in/rad/in) and 926.7 KN-m/rad/m (208.3 kip-in/rad/in), respectively.
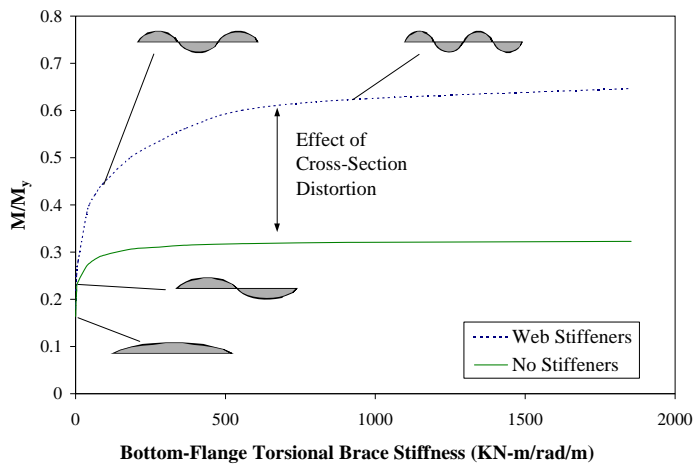
Figure 2.9 Effect of Cross-Section Distortion (Gilchrist, 1997)

17

2.3.5 Effect of Bottom-Flange Lateral Restraint

As discussed in Section 2.2, the lateral moment of inertia of the bottom flange of a U-girder is so large that it acts like a continuous lateral brace. Yura (1993) has shown that the position of a lateral brace along the beam height has a very significant effect on the buckling load. Lateral braces located on the compression flange are the most effective, while ones placed on the tension flange are almost ineffective. The BASP solution in Figure 2.1 verifies that lateral bracing placed on the bottom tension flange provides virtually no increase in buckling capacity.
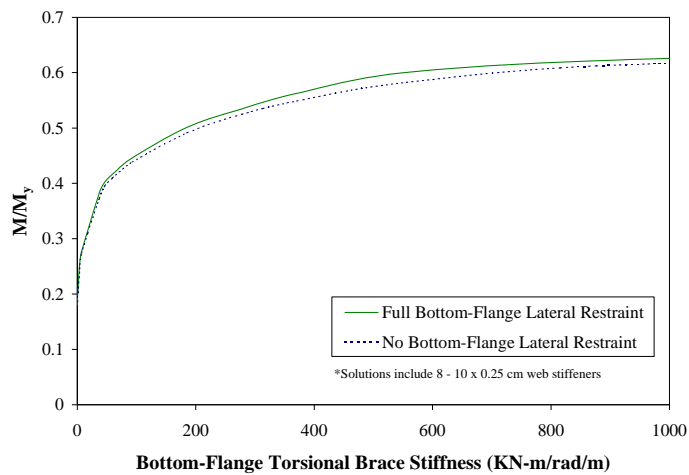
Figure 2.10 Effect of Bottom-Flange Lateral Restraint (Gilchrist, 1997)

18

2.3.6   Effect of Top-Flange Lateral Bracing

Top-flange lateral bracing systems for U-girders can be approximately modeled as discrete lateral springs placed on the top flange of each half-girder. The stiffness of the lateral brace is dependent upon the axial stiffness of the diagonal bracing members, the geometry or size of the brace panels, and whether the bracing system is tension-only or tension-compression.

The boundary conditions for the half-girder model with top-flange lateral bracing are shown in Figure 2.1. Rotational springs were placed at nodes along the length of the bottom flange. Because top-flange lateral bracing forced both flanges to buckle in the same direction, the torsional stiffness calculated was based on the bottom flange bending in reverse curvature (6*EI/b*). The value used for the torsional springs was 843 KN-m/rad/m (190 kip-in/rad/in). In addition, lateral restraints were placed along the bottom flange to prevent any lateral movement of the bottom flange. Again, this was done because the out-of-plane bending stiffness of the wide bottom flange was extremely high. Lateral springs were placed along the top flange of the girder to model the top-flange lateral bracing. By varying their stiffness and spacing, the effect of the top-flange lateral bracing on the buckling behavior was isolated.

Like bottom-flange torsional bracing, top-flange lateral bracing increased the buckling capacity of the girder non-linearly. The amount of increase depended on both the brace stiffness and geometry. For a given number of brace panels, increasing the brace stiffness increased the girder's capacity until buckling between brace points was achieved, as illustrated in Figure 2.1. Unlike bottom-flange torsional bracing, top-flange lateral bracing was not affected by cross-section distortion.

19

Top-Flange Lateral Spring Stiffness, [KN/mm]
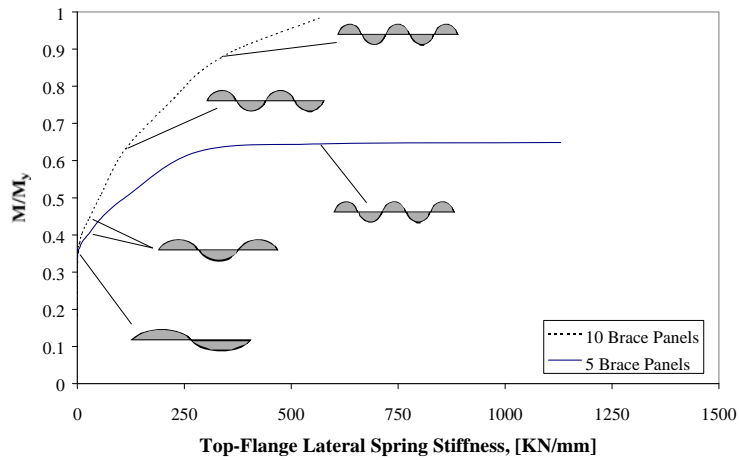
Figure 2.11 Effect of Top-Flange Lateral Brace Stiffness

The torsional restraint provided by the bottom flange caused the first buckling mode to be in two-waves at $M/M_y = 0.32$. As brace stiffness increased, the buckled shape entered intermediate shapes until the ideal stiffness caused buckling between brace points. For the case with five brace panels, the top-flange lateral bracing increased the girder's capacity by 100% to $M/M_y = 0.64$. For the ten brace panel test case, buckling between brace points corresponded to a buckling load greater than the yield load. The yield load for the girder corresponded to a 210% increase in the buckling load.

2.3.7   Effect of Top-Flange Torsional Restraint

The modeling of the top-flange lateral braces as discrete lateral springs was only an idealization of true experimental test conditions. Unlike the analytical model, the actual attachment of the bracing to the top flanges would introduce some level of torsional restraint. The effect of torsional restraint about

20

the strong axis of the top flanges is shown in Figure 2.1. If the top flanges are fully restrained from rotation at each brace point node, the increase in capacity can be substantial. However, at 84 KN-m/rad/node (740 kip-in/rad/node) the girder's response is primarily governed by the top-flange lateral spring stiffness. For comparison, the largest restraint provided by any of the test cases in the experimental program was conservatively estimated to be 8.5 KN-m/rad/node (75 kip-in/rad/node) and was obtained by assuming reverse curvature bending (6EI/L) of the bracing. Therefore, torsional restraint introduced by the lateral bracing was not considered to dominate the buckling behavior of the girder.
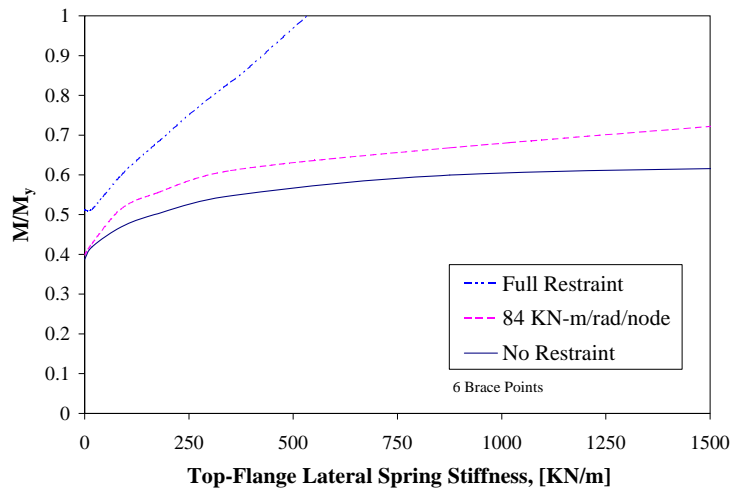
Figure 2.12 Effect of Top-Flange Torsional Restraint

21

CHAPTER 3

Experimental Program

3.1 GENERAL

The experimental program consisted of a series of laboratory experiments designed to study the buckling behavior of U-shaped girders with top-flange lateral bracing. Eighteen tests were conducted in which the girder was confined to the elastic domain. The variable parameters in these tests included brace geometry, stiffness, initial pretension force, and flange connection detail. Following the elastic tests, a final test was conducted to determine the ultimate flexural capacity of the braced girder.

The test girder was 12.19 m (40 ft.) long and simply supported over an 8.53m (28 ft.) span with 1.83 m (6 ft.) overhangs at each end. Loading was applied at the ends of the girder to produce uniform moment between the supports.
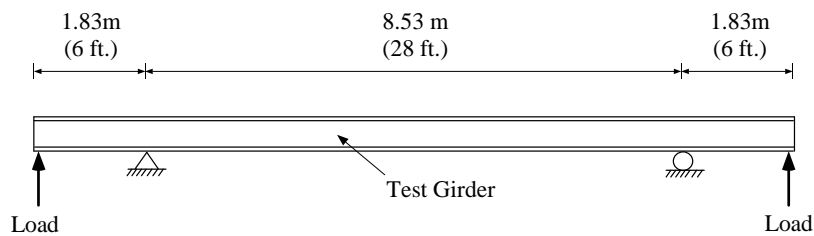
Figure 3.1 Profile of Test Setup (Gilchrist, 1997)

Figure 3.2 Overall Test Setup

3.2   TEST SETUP

3.2.1   Test Specimens

The girder was fabricated using steel with a specified minimum yield stress of 345 MPa (50 ksi) for the top and bottom flanges and 250 MPa (36 ksi) for the webs. Tensile tests were conducted on specimens taken from the girder in accordance with ASTM standards. Average static values were obtained and are summarized in Table 3.1. Additional test information may be found in Appendix A1. The cross-sectional dimensions and properties of the girder are shown in Figure 3.1.

	F_y MPa (ksi)	F_u MPa (ksi)
Top Flange	320 (46)	443 (64)
Web	300 (44)	422 (61)
Bottom Flange	315 (46)	444 (64)

Table 3.1 Tensile Test Data

23

77.62 mm
(3.056 in.)

12.83 mm
(0.505 in.)

6.43 mm
(0.253 in.)

630.25 mm
(24.813 in.)

469.9 mm
(18.5 in.)

16.26 mm
(0.640 in.)

508.76 mm
(20.03 in.)

$A = 1.836 \times 10^4 \text{ mm}^2 (28.46 \text{ in}^2)$

$I_x = 1.11 \times 10^9 \text{ mm}^4 (2676 \text{ in}^4)$

$S_{x_{top}} = 2.54 \times 10^6 \text{ mm}^3 (155.0 \text{ in}^3)$
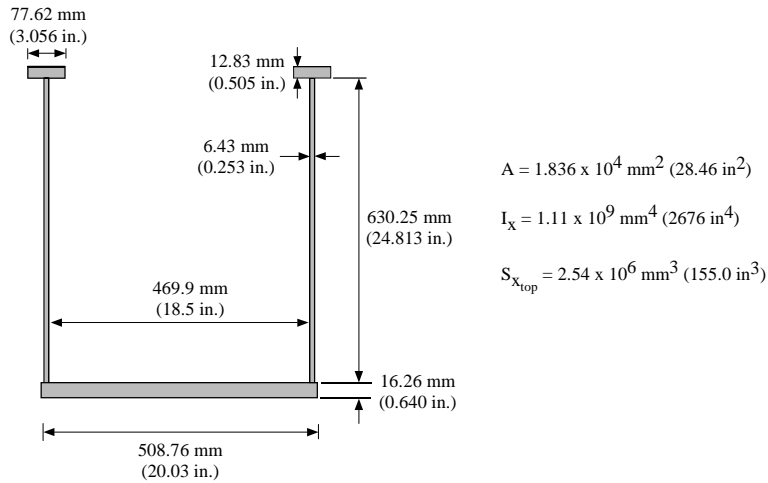
Figure 3.3 Cross-Sectional Properties of Test Specimen (Gilchrist, 1997)

3.2.2   Loading and Support System

The girder supports consisted of two 61 cm (24 in.) long W920 x 223 (W36 x 150) beams oriented perpendicular to the long axis of the U-girder as shown in Figure 3.1. The supports very closely approximated simple support conditions because the webs of the support beams were unstiffened and very slender. If the support beams were conservatively considered fully fixed to the test floor, the rotational stiffness of the support (4*EI/L*) would provide a restraining moment of just 1.3% of the yield moment. Finite element analysis has also shown support restraint to have virtually no influence on the buckling capacity and behavior of the girder (Gilchrist, 1997).

24

Figure 3.4 Support Beam   ***Figure 3.5 Load Ram, Load Cell, and***
                                                    Roller/Bearing Assembly

Load was applied to the specimen 11.43 cm (4.5 in.) from the ends using two hydraulic rams. The rams were connected in parallel to a single pump, ensuring equal force was applied to the girder ends at all times. Roller/bearing assemblies were placed in between the ram and girder so when the girder ends deflected, the line-of-action of the ram force remained vertical.

Four internal stiffening cross-frames were located at each of the support and load points. These internal braces eliminated web crippling and local buckling failure modes at the concentrated load points.

Two external deflection stops were used to limit lateral deflection of the top flanges. These deflection stops, located at midspan and the south quarter point, were frames built around the test girder as shown in Figures 3.8 through 3.10. Outward lateral deflections were controlled by the sides of the frame and inward lateral deflections were controlled by two threaded rods fixed through the frame top.

25

Figure 3.6 X-Brace at Support Location

Figure 3.7 K-Brace at Location of Concentrated Load
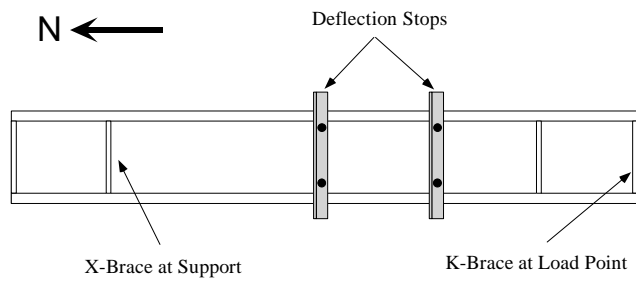
Figure 3.8 Location of Deflection Stops (Plan View of Girder)

Controls Inward Deflection

Controls Outward Deflection
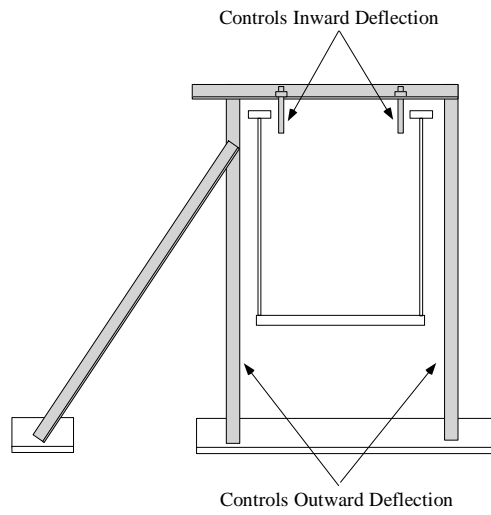
Figure 3.9 Deflection Control of Stop Frames

Figure 3.10 Lateral Deflection Stop Frames

27

3.2.3 Instrumentation

Lateral top flange deflections, midspan vertical deflection, ram load, hydraulic pressure, and brace force strain data were collected using a computerized data acquisition system. Lateral deflections of both top flanges were also monitored using transits. The midspan vertical deflection was measured using an electronic linear displacement potentiometer that had an accuracy of 0.0254 mm (0.001 in.). This measurement was taken to verify that the girder remained in the elastic range during testing.

The lateral deflections of the east top flange were measured using electronic linear displacement string potentiometers as shown in Figure 3.1. The string pots were mounted at flange level more than 0.9 m (3 ft.) away to minimize the effect of vertical displacement of the girder during loading. The gages had an accuracy of 0.0254 mm (0.001 in.). The points along the top flange that were measured varied with the each particular test case.

String Potentiometer
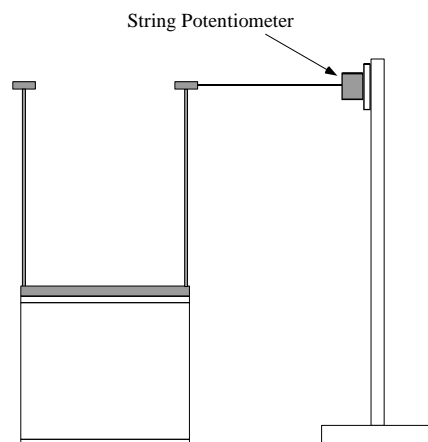
Figure 3.11 Top-Flange Lateral Displacement Gages

28

The lateral deflections of both flanges were also measured using transits located at one end of the specimen as shown in Figure 3.2. The transits were sighted parallel to the two supports. The lateral deflection readings were used to produce deflected shapes of the top flanges. The accuracy of these readings was 1.0 mm (0.04 in.).
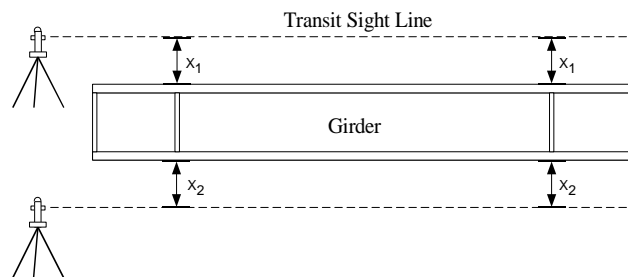
Figure 3.12 Transit Locations (Plan View)

Loads were obtained from load cells placed in series with each of the rams and the girder as shown earlier in Figure 3.2. The load cells had a capacity of 444.8 KN (100 kips) and a maximum absolute error of 0.63%. Hydraulic ram pressure was monitored using a pressure transducer as a secondary measure of the applied load.

3.3   BRACING SYSTEM

The top-flange lateral bracing system was a tension-only X-brace system placed within the constant moment region between supports. Figure 3.1 shows a test case with five brace panels. The end brace points were located 76.2 mm (3

in.) to the interior of the support cross frames. All other brace points were evenly
spaced to produce equal sized brace panels.
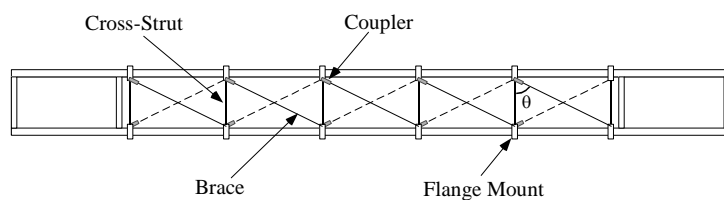
Figure 3.13 Tension-Only Bracing System

3.3.1   Braces

The braces, with the exception of the final test case, were fabricated using
T6061-T6 and T6063-T1 aluminum flat bars with moduli of elasticity of 69,000
MPa (10,000 ksi) and specified yield stresses of 260 MPa (38 ksi) and 150 MPa
(22 ksi), respectively. Aluminum was the material of choice because of its high
strength and low relative stiffness when compared to steel. Depending on the test
case, the sizes varied from 3.175 mm x 12.7 mm (1/8 in. x 1/2 in.) to 6.35 mm x
25.4 mm (1/4 in. x 1 in.) wide. Cross-strut braces which connected directly
opposite points on the two flanges were made from 12.7 mm x 19.05 mm (1/2 in.
x 3/4 in.) aluminum bars. All diagonal braces and cross-struts were T6061-T6
grade aluminum except the 3.175 mm x 12.7 mm (1/8 in. x 1/2 in.) bars, which
were a T6063-T1 alloy.

The final test case used 3.175 mm x 12.7 mm (1/8 in. x 1/2 in.) A36 steel
flat bars. Steel braces were used in this test case because the connection detail
required welding the braces directly to the top flanges of the girder.

3.3.2 Connection to Flange

Three mounting schemes were used to attach the braces to the top flanges of the girder. The original flange mount connection was designed so the attachment to the flanges was not permanent, allowing for easy variation of the brace geometry or number of brace points. Subsequent tests modified the original design to isolate the effects of particular test parameters.

The original connection design attached the braces and couplers to the flanges of the girders using removable flange mounts. The mounts, which were machined from T6061-T6 aluminum, gripped the flanges with two opposing set screws, as shown in Figure 3.1. This design connected the diagonal braces and cross-struts at the same pin location, but had a 76.2 mm (3 in.) eccentricity from the flange centroid.
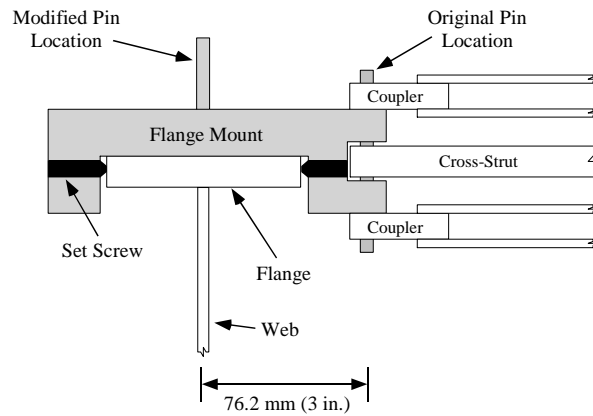
Figure 3.14 Original and Modified Flange Mount Connection (Profile)

31

Figure 3.15 Original Brace, Coupler, and Flange Mount Connection

The modified connection detail, also shown in Figure 3.1, moved the pin location from its eccentric position to the center of the flange. The purpose of this detail change was to investigate the effect of out-of-plane flange rotations on the brace behavior. The final connection detail, shown in Figure 3.1, involved directly welding the braces to flange of the girder. The flange mounts were still used to connect the cross-struts. The purpose of this detail was to investigate the effect of connection stiffness on the brace behavior.

3.3.3 Brace Force Measurement

Strain gages were used to obtain forces in all the brace members. Gages were placed directly on the cross-strut members and on the diagonal brace members with the modified and welded connections. For diagonals attached with the original flange mount connection, brace forces were acquired by placing a coupler device that was strain gaged in series with the braces as shown in Figure 3.2.
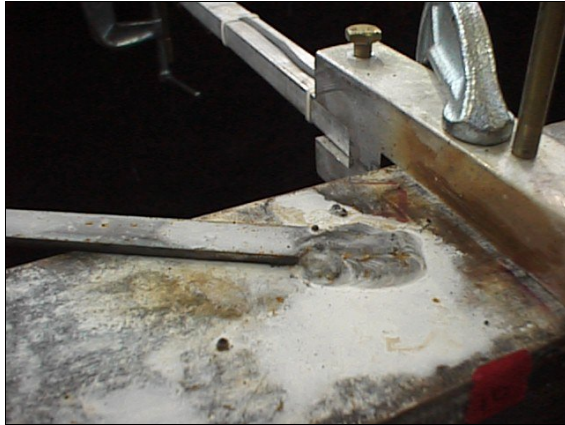
Figure 3.16 Welded Brace Connection Detail

Strain Gage

Vertical Pin

Horizontal Screw
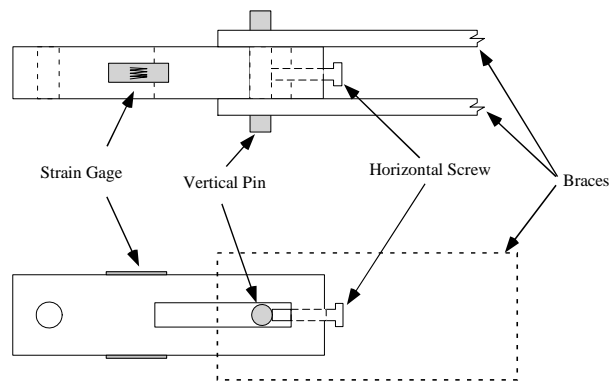
Braces

Figure 3.17 Coupler-Brace Connection

The coupler was designed as a bolted splice connector. One end was bolted to the flange mount and the other was bolted to two diagonal braces for symmetry. The vertical pin shown in Figure 3.2 connected the braces to the

coupler. This pin pressed against a horizontal screw in the coupler. Tightening this screw removed any slack or introduced pretensioning in the braces prior to girder loading. As force developed in the brace, the vertical pin was free to pivot as illustrated in Figure 3.3. This assured equal force in each brace. The design also allowed for only tensile force transfer because any compressive movement would cause the vertical pin to slide within the coupler.
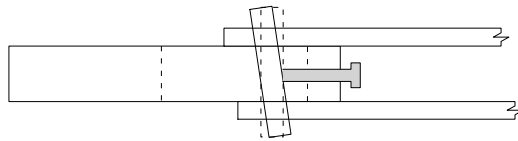
Figure 3.18 Rotational Freedom of Coupler Pin Allows Force Redistribution

3.3.4   Coupler Calibration

To obtain diagonal brace forces, two strain gages were placed on the opposite sides of each coupler, as shown in Figure 3.2. If the cross-section of the couplers were uniform, the brace force would easily be obtained by:

$$F_{brace} = E \cdot A \cdot \varepsilon \tag{3.1}$$

where F_{brace} is the brace force, E is the modulus of elasticity, A is the cross-sectional area of the coupler, and ε is the average strain from the gages. However, because the cross-sections were not uniform, Equation (3.1) did not produce the correct brace force. Therefore, calibration of the couplers was necessary.

The couplers were calibrated in a universal testing machine to determine the force associated with a given strain gage output. A typical calibration plot is shown in Figure 3.1. A linear regression analysis was used to calculate the calibration factor for each coupler. This calibration factor was used in place of

the product of *E* and *A*. Both the loading and unloading data were used in the regression analysis. The average calibration factor was 140% greater than the product of *E* and *A*. A summary of the calibration factors for all the couplers is listed in Appendix A2.
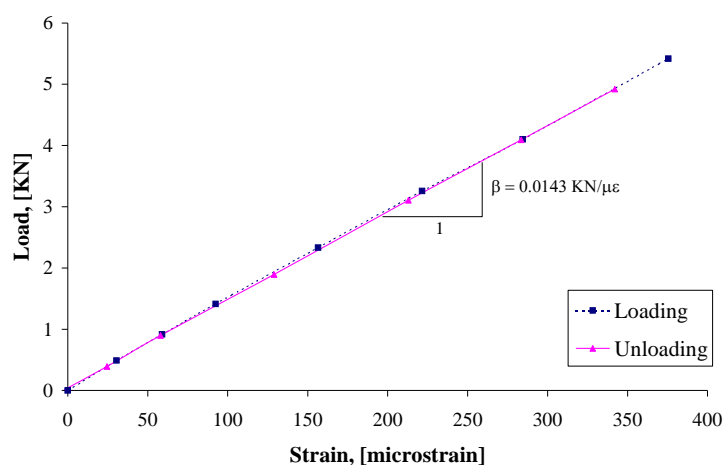
Figure 3.19 Typical Strain Gage Calibration Curve

Since the couplers were connected in series with the diagonal bracing, the stiffness of the couplers affected the overall stiffness of the diagonal bracing system. The stiffness of the couplers was obtained by using the force-displacement measurements from the universal testing machine tests. A typical force versus displacement plot is shown in Figure 3.2. The stiffness at lower load levels was markedly different than at higher load levels. Because the brace forces in all of the experimental test cases that used the couplers did not exceed 1.6 KN

35

(350 lbs.), the calculation of stiffness was based on load levels less than this value.   The data points used in the regression analyses for the loading and unloading stages are indicated by the bold data points in Figure 3.2.   The two stiffness values obtained were then averaged to produce the coupler's stiffness. The average stiffness obtained from the various calibration tests was found to be 4.4 KN/mm (25 kips/in).
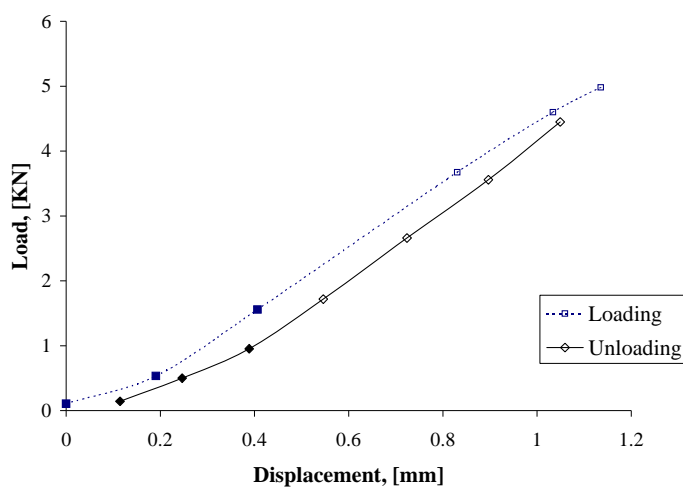
Figure 3.20 Typical Coupler Force vs. Displacement Response

3.4   TEST VARIABLES

There were several variable parameters that were considered in the scope of this experimental program.   These parameters were brace geometry, brace stiffness, initial brace pretension force, and connection detail.

36

3.4.1 Brace Geometry

The brace geometry was based on the number of brace panels located between the supports. The brace angle, θ, was the angle between the diagonal brace and perpendicular cross-struts (see Figure 3.1). Three brace geometry cases were examined: four, five and ten brace panels.

3.4.2 Brace Stiffness

The effective lateral brace stiffness was dependent on both the brace geometry and the axial stiffness of the braces used. The axial stiffness, β_{axial}, of a tension member was:

$$\beta_{axial} = \frac{EA}{L} \tag{3.2}$$

where E was the modulus of elasticity, A was the total cross-sectional area of the all the bars in a diagonal, and L was the length of the brace. When the coupler was placed in series with the diagonal braces, the stiffness of the brace system was equivalent to the stiffness of two springs in series. The cosine function was necessary to convert the diagonal brace to an equivalent brace perpendicular to the flanges. The equivalent lateral stiffness of a diagonal brace was then:

$$\beta = \left(\frac{\beta_{axial}\beta_{coupler}}{\beta_{axial} + \beta_{coupler}} \right) \cos^2 \theta \tag{3.3}$$

3.4.3 Brace Pretension Force

The horizontal screw on the couplers allowed the initial tension in the diagonal braces to be selected. In most of the test cases, the horizontal screw was hand tightened to remove any slack in the braces after installation. In a few cases, the coupler screw was tightened an additional amount before any load was applied to the girder to create a pretension force in the braces.

37

3.4.4   Connection Detail

The three connection details described in Section 3.3.2 were used to investigate their effect on the bracing system and girder's buckling behavior. The modified detail with the pin located at the center of the flange investigated the effect of flange rotations on the effectiveness of the diagonal braces while the welded connection detail investigated the effect of the previous details on the brace stiffness.

A top-flange lateral bracing system attempts to control the relative movements of adjacent brace points. In a tension-only system, the braces are effective only when the end points where they are attached move apart. Figure 3.1 shows how the relative lateral translation of adjacent brace points along the top flange cause the diagonal lengths to change.
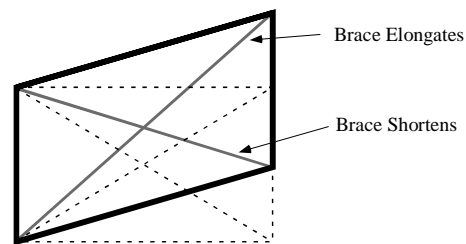
Figure 3.21 Brace Length Change Due to Flange Lateral Translation

The original location of the pin connection point between the diagonal braces, cross-struts, and flange mounts was 76.2 mm (3 in.) to the interior of the center of the top flange. The rotation of the flanges associated with buckling might have contributed to the relative movement of the brace ends due to the mount eccentricity and is illustrated in Figure 3.2. In order to investigate the

38

contribution of this rotational effect, the pin location was moved to the center of the flange in later tests (see Figure 3.1). The eccentricity of the brace-mount connection also introduced torsional restraint to the top flanges. As discussed in Section 2.3.7, torsional restraint of the top flanges had a negligible effect on the buckling behavior of the girder.

Brace Elongates

Brace Shortens
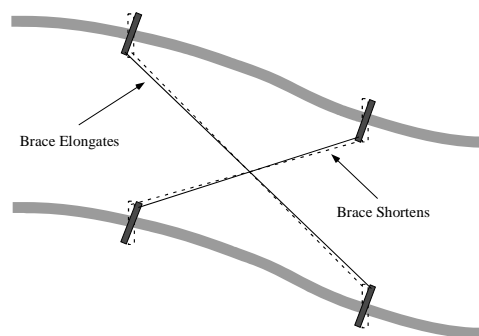
Figure 3.22 Brace Length Change Due to Flange Rotation

During some of the test runs, the forces in the diagonal braces caused the flange mounts to rotate about their long axis. This slight movement may have decreased the stiffness of the diagonal bracing system to a degree where they became inadequate. In order to verify this, a test case was conducted in which the braces were welded directly to the flanges. This connection detail ensured no loss of stiffness from movement at the connection mount and provided a high level of confidence that the theoretical brace stiffness was equal to the experimental brace stiffness.

3.5   TEST CASES

The test cases used in the experimental program were initially chosen based on the results from BASP analysis and are summarized in Table 3.1. As testing progressed and results were obtained, the test cases were modified. Some variables thought to have an influence on the results did not. Cases were then developed to isolate the critical parameters governing the girder's response.

The test identifier designates the number of brace panels between the supports as well as the test run number. For example, test RU-2 refers to the second test run for the unbraced rectangular girder while R5-3 refers to the third test conducted using five brace panels. The brace angle, θ, is the angle between the diagonal brace and perpendicular cross-strut, as shown earlier in Figure 3.1. The ideal brace stiffness was the value obtained from BASP analysis that caused buckling between brace points and serves as a reference value.

The first test case, RU-1, determined the experimental unbraced buckling capacity of the girder. During test R4-4, some yielding occurred in the top flanges, so a second unbraced case was conducted to determine if the buckling capacity had been affected. Tests R10-4 through R10-W were conducted to determine the ultimate strength of the girder. Near the final stages of loading test R10-4, a brace mount slipped from its attachment to the flange. Therefore, an additional test, R10-5, was conducted. Test R10-W employed the welded connection detail. This test failed the girder.

40

Test	Brace Angle, θ	Brace Stiffness		Couplers	Pin Location	Pretension	Comments
	degrees	KN/mm	x Ideal				
RU-1	-	-	-	-	-	-	
RU-2	-	-	-	-	-	-	After flange yielding in R4-4
R4-1	81.4	0.11	0.4	Yes	Offset	-	
R4-2	81.4	0.11	0.4	Yes	Offset	Yes	
R4-3	81.4	0.11	0.4	Yes	Offset	Yes	
R4-4	-	-	-	-	-	-	Only cross-struts
R4-5	81.4	0.33	1.2	Yes	Offset	-	
R5-1	-	-	-	-	-	-	Only cross-struts
R5-2	79.3	0.75	0.7	Yes	Offset	-	
R5-3	79.3	0.75	0.7	Yes	Offset	Yes	
R5-4	79.3	1.28	1.2	Yes	Offset	-	
R5-5	74.3	2.09	2.0	No	Center	-	
R5-6	74.3	2.09	2.0	No	Center	-	
R5-7	74.3	1.31	1.2	Yes	Center	-	
R5-8	74.3	0.42	0.4	Yes	Center	-	
R10-1	60.7	5.53	5.3	No	Center	-	
R10-2	60.7	5.53	5.3	No	Center	-	
R10-3	60.7	5.53	5.3	No	Center	-	
R10-4	60.7	5.53	5.3	No	Center	-	
R10-5	60.7	5.53	5.3	No	Center	-	
R10-W	60.7	4.36	4.0	No	-	-	Welded connection

Table 3.2 Summary of Test Cases

3.6   TEST PROCEDURE

Load was applied to the girders in deflection-controlled incremental stages. Each load increment was selected by monitoring the point of maximum lateral deflection of the top flange. At each increment, a computerized data acquisition system was used to record the instrumentation data. This included load cell, pressure transducer, strain gage, and displacement potentiometer data. Periodically, the deflected shapes of the top flanges were recorded using the two transits as described in Section 3.2.3.

For the elastic tests, loading continued until the stresses in the top flanges were close to yield. This was achieved by monitoring both the applied load and the maximum lateral deflection. The first-order compressive stress was calculated using the applied moment and girder section modulus. The maximum second-order stress was based on the point of maximum lateral deflection. By keeping the sum of the first and second order stresses below yield, the test was confined to the elastic range. Whitewash applied to the top flanges provided a visible method for detection of yielding and was monitored periodically during the tests.

CHAPTER 4

Test Results

4.1   DETERMINATION OF BUCKLING LOADS

The rectangular U-girder used in the experimental program was designed to buckle elastically, which means the top flanges of the girder would buckle at loads less than the yield moment, M_y. This allowed multiple test cases to be run on the same girder without causing any permanent deformation. The top flanges, however, were not perfectly straight and had initial imperfections. Load applied to the girder would cause lateral deflection of the top flanges. The additional P-Δ moments added to the in-plane bending stresses could lead to yielding of the flanges at load levels less than the buckling load. In order to keep the girder in the elastic range and still obtain the girder buckling loads, an extrapolative load-deflection plotting technique was used.

4.1.1   Southwell Method

Southwell (1932) developed a method to predict the buckling load of initially imperfect columns without having to test the column to failure. By plotting the results of a column test in a certain manner, it would be possible to determine that a column's buckling load was, for example, 100 KN (22.5 kips) even though the maximum load reached during the test was 85 KN (19.1 kips).

The typical behavior of a column in the form of load versus mid-height deflection is shown in Figure 4.1. Perfect columns with no initial out-of-straightness exhibit no lateral deflection at load levels less than the Euler buckling load. For columns with small initial imperfections there is some lateral deflection that occurs before the Euler load is attained. The P-Δ moments in columns with

43

large initial imperfections will cause yielding before the elastic buckling load can
be reached.
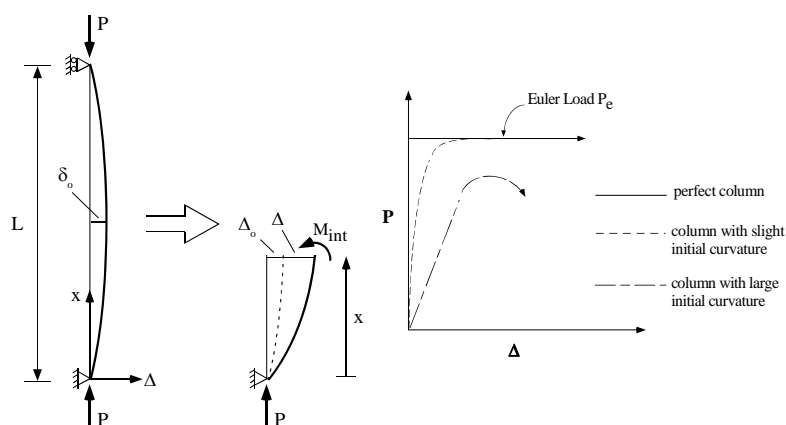
Figure 4.1 Buckling of Imperfect Columns

Southwell assumed the initial shape of the column to be a half-sine wave
with an initial imperfection at mid-height equal to δ_o. The equation for the initial
shape is characterized by

$$\Delta_0(x) = \delta_o \sin\left(\frac{x\pi}{L}\right)$$ (4.1)

The load-deflection relationship based on this initial shape can then be
approximated (Timoshenko, 1961) as

44

$$\Delta_{Total} = \Delta_0 + \Delta = \left(\frac{1}{1 - P/P_e} \right) \cdot \Delta_0 \qquad (4.2)$$

where Δ_{Total} is the total lateral deflection, Δ the lateral deflection from the initial shape, P is the axial load in the column, and P_e is the Euler buckling load. Solving in terms of Δ yields

$$\Delta = \frac{P}{P_e} \left(\frac{\Delta_o}{1 - P/P_e} \right) \qquad (4.3)$$

and rearranging further gives

$$\frac{\Delta}{P} = \frac{1}{P_e} \Delta + \frac{\Delta_o}{P_e} \qquad (4.4)$$

By considering Δ/P and Δ as variables, Equation (4.4) takes the form of the equation of a straight line and can be plotted as shown in Figure 4.2. This Southwell plot produces a linear relationship within the elastic range. The inverse slope of the data represents the predicted buckling load. The variable, Δ, is not the absolute deflection, but the deviation from the initial shape and can easily be measured in the laboratory. The accuracy of this method increases as the maximum test load approaches the actual buckling load, or the ratio P/P_e approaches the value of 1.0. Predicted buckling loads are within 5% for $P/P_e \geq 0.6$ and within 2% for $P/P_e \geq 0.8$ (Southwell, 1932).
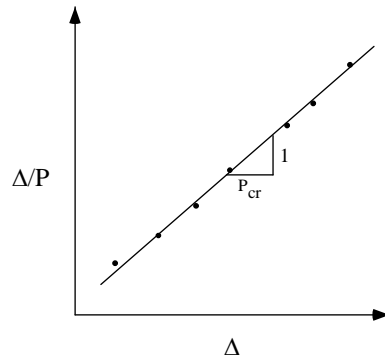
Figure 4.2 Southwell Plot (Gilchrist, 1997)

The Southwell method can only be applied to members in the elastic range. The method also depends on the assumption that the final buckled shape is of the same mode as the initial shape. In cases where this does not occur or where the deflection is very small, the Southwell plots will produce very errant results (Gilchrist, 1997). For example, consider the case of a column braced at mid-height with a single-wave initial imperfection as shown in Figure 4.3. Initial loading of the column will cause deflection to continue in the one-wave shape. However, if loading is continued and the brace is adequate, the column will buckle into two-waves. If lateral deflection for this case is measured at the first quarter point, the initial deflection readings will be in one direction but subsequent readings will be in the opposite direction. This difference in initial and final shapes produces poor Southwell plots, an example of which is shown in Figure 4.4.

46
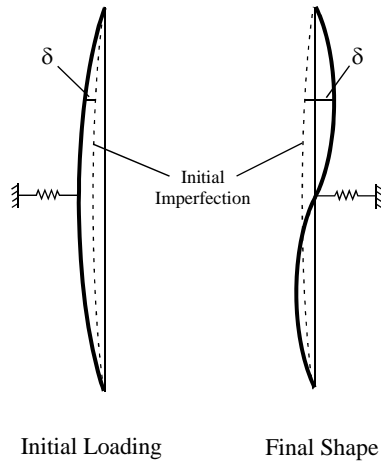
Figure 4.3 Deflection Reversal when Initial and Final Shapes are Different
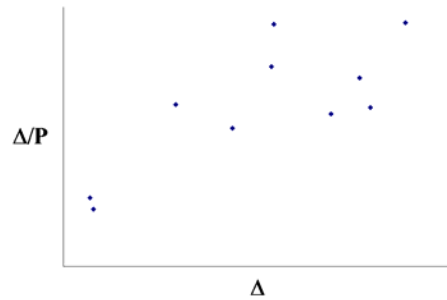
Figure 4.4 Typical Poor Southwell Plot

The Southwell plotting method is not limited only to columns. The scope of application includes any type of buckling problem where there is a hyperbolic load-deflection response similar to Equation (4.2). It is only necessary to have data relating load to a deformation characteristic such as deflection, rotation, or

47

twist. Trahair (1969) and Meck (1977) successfully applied this method and variations of it to predict buckling loads for beams.

4.2   INITIAL IMPERFECTIONS

Before load was applied to the girder, the initial imperfections of the top flanges of the girder were recorded. Measurements were made using two transits sighted parallel to the two supports as described in Section 3.2.3.   The imperfections for the east and west flanges are shown in Figure 4.1 and Figure 4.2, respectively
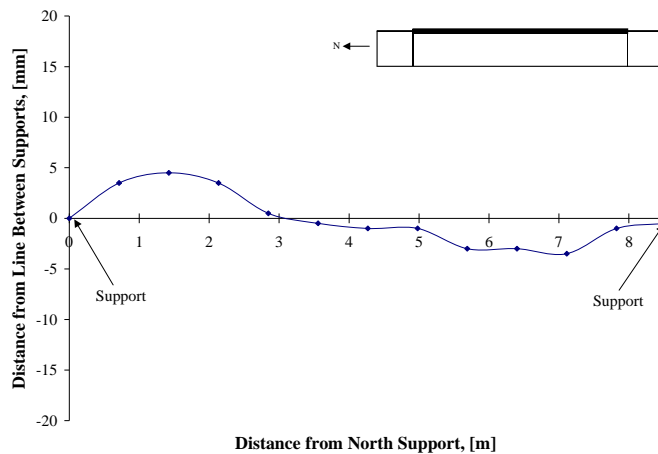
Figure 4.5 Initial Imperfections of East Flange

48
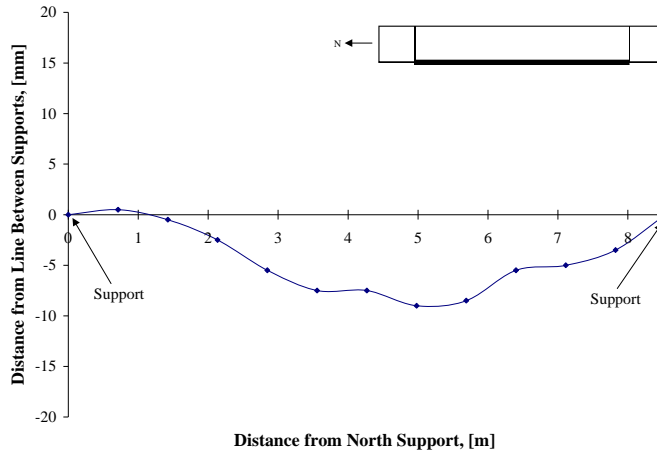
Figure 4.6 Initial Imperfections of West Flange

Out-of-straightness values for each test case were calculated by dividing the relative lateral displacement between brace points, Δ_o, by the brace panel size, s. The results are summarized in Table 4.1.

Test Case	Δ_o/s
Unbraced	0.0010 (1/900)
4 Brace Panels	0.0030 (1/330)
5 Brace Panels	0.0038 (1/260)
10 Brace Panels	0.0060 (1/167)

Table 4.1 Maximum Out-of-Straightness of Brace Panels

Out-of-straightness values for specific brace panels in each of the brace geometry cases can be found in Appendix A3.

49

4.3   DETERMINATION OF BRACE FORCES

The brace forces for the elastic tests were obtained by using the strain-gaged couplers described in Section 3.3.3. For the inelastic tests, strain gages were placed directly on selected diagonal brace members. Brace forces are typically normalized by the load necessary to cause buckling between braces. However, this value changed with each brace geometry and, in the case of ten brace panels, exceeded the girder's yield strength. To maintain consistency, the diagonal brace forces, F_{br}, and the cross-strut forces, F_{xs}, were normalized as a percentage of the force necessary to cause yielding in both girder flanges. The flange yield force, F_{yf}, was calculated as the product of the specified minimum yield stress of the flanges, 345 MPa (50 ksi), and the area of both flanges and was equal to 686.4 KN (154.3 kips).

4.4   ELASTIC GIRDER TESTS

A series of eighteen tests were conducted in which the girder was confined to the elastic domain. The purpose of these tests was to investigate the increase in buckling strength provided by the top-flange lateral bracing with different brace stiffnesses and geometries. This test series included no bracing, four, five, and ten brace panel test cases. Inspection of the whitewashed top flanges during the tests provided a visible verification of elastic behavior.

4.4.1   Buckling Loads

Southwell plots were created using load-deflection data from the string potentiometers measuring lateral deflection of the girder's top flange. A typical Southwell plot is shown in Figure 4.1. A linear regression analysis was used to calculate the slope of the trendline through the data points. The inverse of the slope of this line is the predicted Southwell elastic buckling load, P_{cr}. The data

points chosen for use in the regression analysis were the last several data points recorded. The number of data points used was based on providing an R-squared value greater than 0.9975. This was done to ensure a sufficient number of data points was used in the regression analysis and to maintain consistency in data sampling between the test cases.
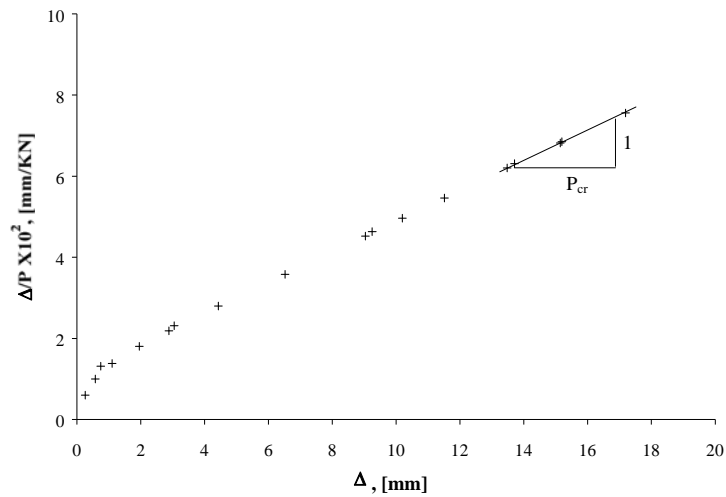
Figure 4.7 Typical Southwell Plot

During the beginning stages of each test, the data points do not align with the linear portion near the latter test stages. This is due in part to uplift of the girder and settlement of fixtures and braces during the initial loading. The deviation can be mostly attributed to the fact that when P/P_e is small, the higher order terms that were neglected in the approximate solution of Equation (4.2) no longer have negligible effects (Bažant, 1991). That is, Equation (4.2) was derived

51

using a Fourier sine series characterization for the initial deflected shape. When P/P_e is not small, the leading term in the series dominates the response, while the higher order terms have only a negligible contribution. This leading term is the expression seen in Equation (4.2).

To maintain consistency, lateral deflection data used to calculate the Southwell buckling loads was measured from the same location on the top flange. The Southwell method typically yields better results with data based on larger deflections. Therefore, the potentiometer chosen was near the point of maximum lateral deflection. This point, shown in Figure 4.2, was 3.2 m (10.5 ft.) from the south support and was near the point of maximum deflection for all test cases.
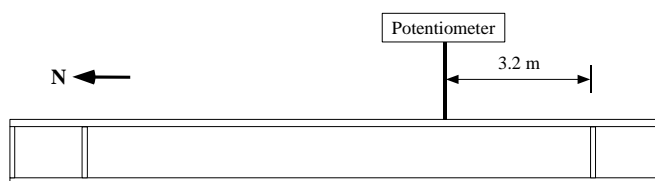
Figure 4.8 Potentiometer Used for Southwell Displacement Data

Table 4.1 provides a summary of the Southwell predicted buckling loads. Applied test loads and buckling loads are reported in terms of the ram force, *P*, which is directly proportional to the stress in the top flanges. Reported values are normalized by P_y, the ram load necessary to cause yielding in the top flanges based on simple elastic bending theory. The value for P_y was equal to 478.7 KN (107.6 kips).

During test R4-4, some yielding occurred that was visibly observed in the whitewashed top flanges. The permanent set of the top flanges was recorded and can be found in Appendix A4. An additional test, RU-2, was conducted to see if

52

the yielding had affected the buckling strength of the unbraced girder. The results indicated a slight decrease in the predicted Southwell buckling load from $0.50P_y$ to $0.47P_y$.

Test Case	Maximum Applied Test Load (P_{max}/P_y)	Southwell Predicted Buckling Load (P_{cr}/P_y)
RU-1	0.415	0.50
RU-2	0.415	0.47
R4-1	0.475	0.58
R4-2	0.458	0.54
R4-3	0.467	0.55
R4-4	0.476	0.54
R4-5	0.453	0.54
R5-1	0.426	0.53
R5-2	0.425	0.58
R5-3	0.427	0.58
R5-4	0.421	0.55
R5-5	0.443	0.58
R5-6	0.447	0.59
R5-7	0.410	0.56
R5-8	0.418	0.57
R10-1	0.511	0.73
R10-2	0.509	0.89
R10-3	0.490	0.81

Table 4.2 Southwell Predicted Buckling Loads

4.4.2 Buckled Shapes and Brace Behavior

Figures 4.9 through 4.12 show the typical buckled shapes of the top flanges between the two supports for the various brace geometries. The braces were visually inspected during each test to determine whether they were engaged, slack, or buckled. Engaged diagonal braces are denoted by bold lines, while buckled or slack braces are shown as dotted lines.

The final buckled shape for all of the brace geometries and stiffness cases was two-waves between the supports. The flanges of the unbraced girder buckled independently of one another because cross-struts were not present to maintain the distance between flanges.
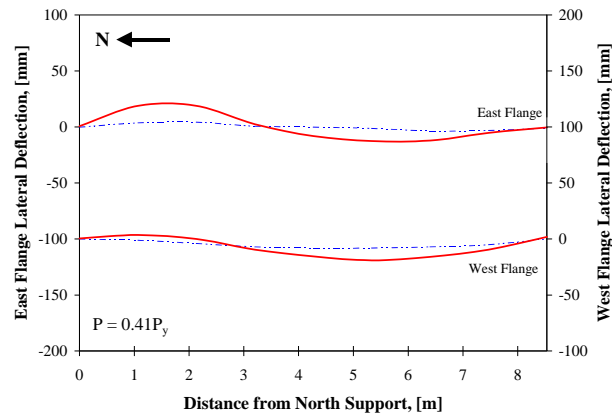
Figure 4.9 Typical Buckled Shape for Unbraced Girder
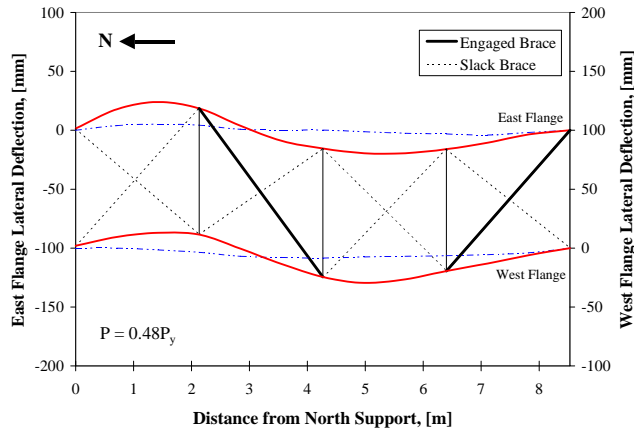
Figure 4.10 Typical Buckled Shape for 4 Brace Panels
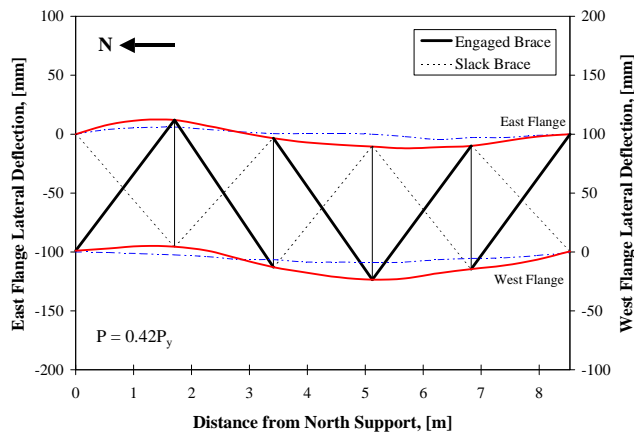
Figure 4.11 Typical Buckled Shape for 5 Brace Panels
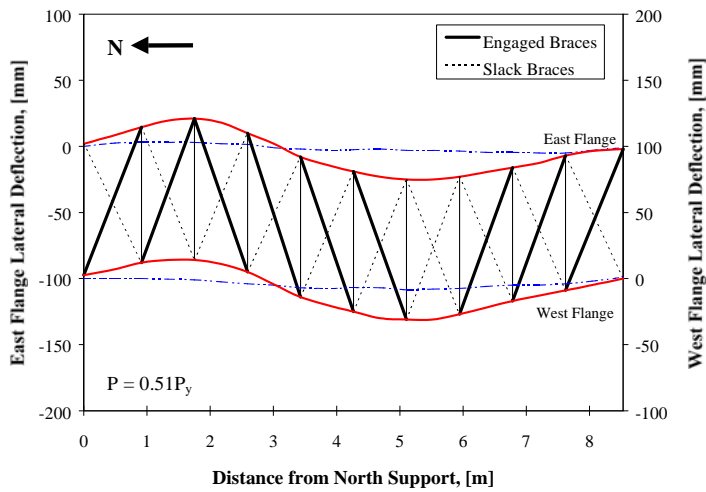
Figure 4.12 Typical Buckled Shape for 10 Brace Panels

During the beginning stages of loading, all of the diagonal bracing visibly slackened from their initially taught position as shown in Figures 4.13 and 4.14. This was observed in all of the test cases and was especially apparent in the cases with fewer brace panels. The shortening of the top compression flange under loading caused the bracing to slacken. As the top flanges began to deflect laterally, some braces engaged to prevent the panel distortion while others remained slack. As an example, the second brace panel from the north in the four brace panel case had a diagonal brace engage as the panel attempted to distort (Figure 4.2). However, the adjacent brace panel to the north also distorted, but the diagonal brace did not engage. The lateral deflection or panel distortion necessary to elongate the brace in the first panel was not sufficient to make up for the slack that was introduced when the brace panel shortened.

56

Figure 4.13 Bracing Taught Before Loading

Figure 4.14 Bracing Slack During Initial Loading

4.4.3   Brace Forces

The general distribution of brace forces was very similar within each brace geometry case. Typical brace force distributions for the four and five brace panel test cases are shown in Figures 4.15 and 4.16. The diagonal brace P2a in both the

four and five brace panel test cases attracted the highest brace forces. As visually observed during the tests, the number of braces that developed significant forces increased as the number of brace panels increased. The four brace panel test cases had only two active braces while the five brace panel cases typically had five. A summary of the maximum brace forces reached in each test is shown in Table 3.1. A dash indicates those particular brace forces were not measured during a given test.

Test Case	P_{max}/P_y	Diagonal Braces (F_{br}/F_{yf})	Cross-Struts (F_{xs}/F_{yf})	
		Tension	Tension	Compression
R4-1	0.48	0.23%	0.41%	-0.11%
R4-2	0.46	0.24%	0.25%	-0.12%
R4-3	0.47	0.29%	0.34%	-0.13%
R4-4	0.48	-	0.61%	-0.13%
R4-5	0.45	0.27%	0.33%	-0.03%
R5-1	0.43	-	0.26%	-0.10%
R5-2	0.42	0.17%	0.22%	-0.34%
R5-3	0.43	0.19%	0.23%	-0.33%
R5-4	0.42	0.11%	0.18%	-0.34%
R5-5	0.44	-	-	-
R5-6	0.45	-	-	-
R5-7	0.41	-	-	-
R5-8	0.42	0.11%	0.18%	-0.20%
R10-1	0.42	-	0.53%	-0.40%
R10-2	0.51	-	0.51%	-0.28%
R10-3	0.49	-	0.54%	-0.31%

Table 4.3 Maximum Brace Forces for Elastic Tests

58
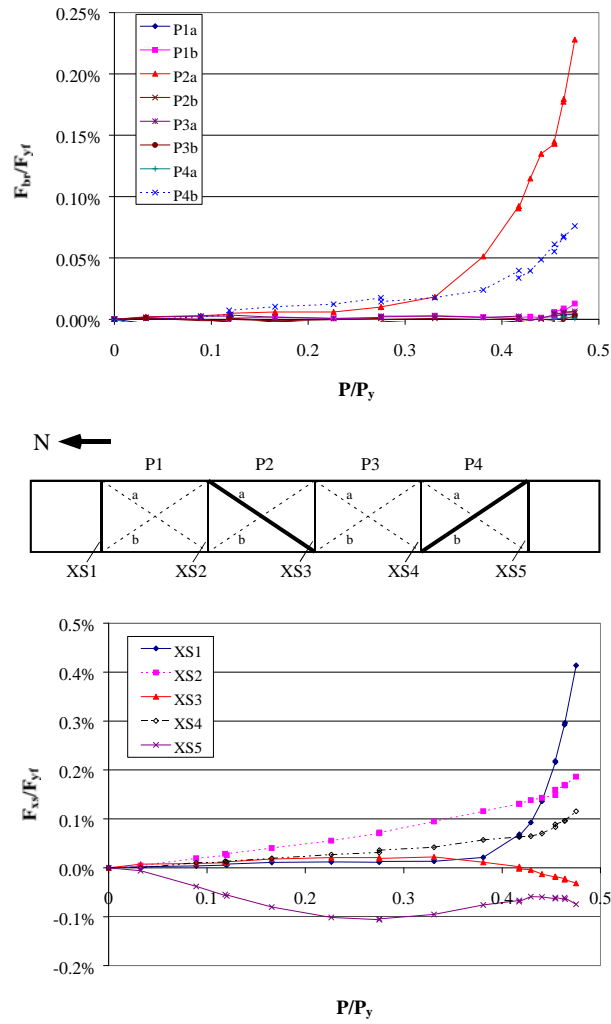
Figure 4.15 Typical Brace Force Distribution for 4 Brace Panels

59
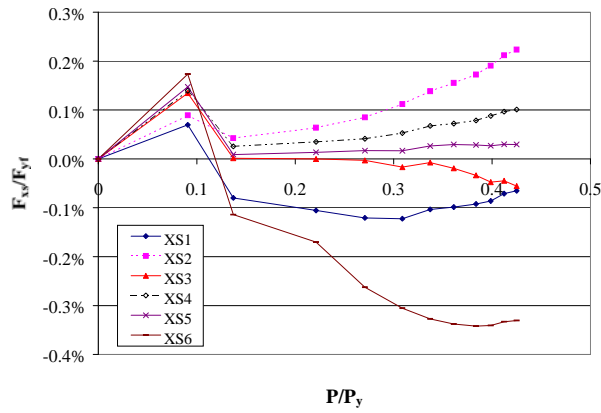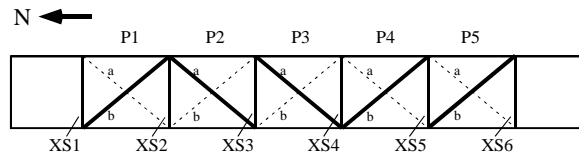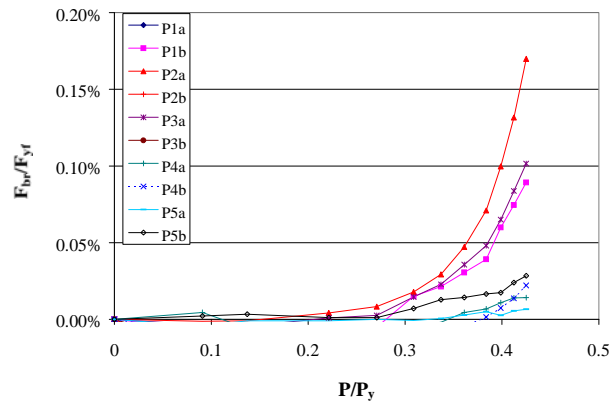
Figure 4.16 Typical Brace Force Distribution for 5 Brace Panels

60

4.5 INELASTIC GIRDER TESTS

A series of three tests were performed in which the girder was taken into the inelastic range. The goal of these tests was to obtain the true maximum load carrying capacity of the braced girder.

4.5.1 Tests R10-4 and R10-5

The purpose of tests R10-4 and R10-5 was to verify the accuracy of the predicted Southwell buckling loads obtained from the elastic girder tests. During the final stages of loading for test R10-4, a brace mount slipped from the top flange, causing premature termination of the test. Therefore, a second test, R10-5, was conducted to verify the maximum load carrying capacity of the girder.

Before test R10-5 was conducted, the slight permanent set of the top flanges caused by the previous test was recorded and can be found in Appendix A6. Results from test R10-4 were very similar to R10-5 and may be found in the Appendix A5.

The load versus lateral deflection response for R10-5 is shown in Figure 4.1. Lateral deflection data was recorded from the same linear string potentiometer as the elastic girder tests and was located near the point of maximum lateral deflection. The load-deflection response indicates the maximum load carrying capacity of the girder was reached because lateral deflection occurred with very little increase in load. Also, the deviation of the load versus midspan vertical deflection from linear indicates inelastic behavior, which was visibly observed by yielding in the whitewashed top flanges. The maximum load achieved was only $0.55P_y$. By contrast, the Southwell predictions for this test (from R10-1 through R10-3) varied between $0.73P_y$ and $0.89P_y$.

61
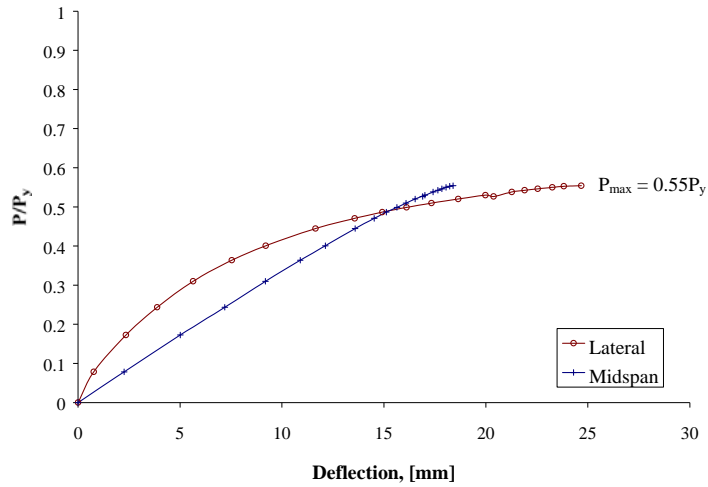
Figure 4.17 Load-Deflection Response for Test R10-5

The brace forces measured included three diagonal braces and six cross-struts and are shown as the heavy lines in Figure 4.2. The location of the instrumented members are denoted by the heavy dashed lines in the plan view. The maximum diagonal brace force reached was 0.82% of the flange yield force, while the maximum cross-strut force reached 0.53% in compression and 0.23% in tension.
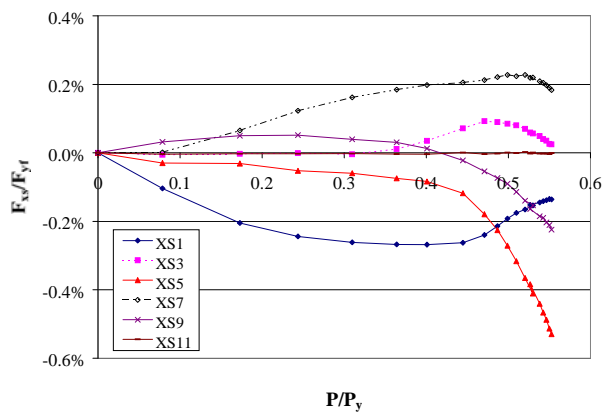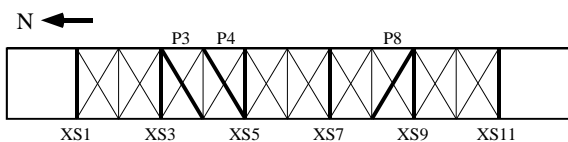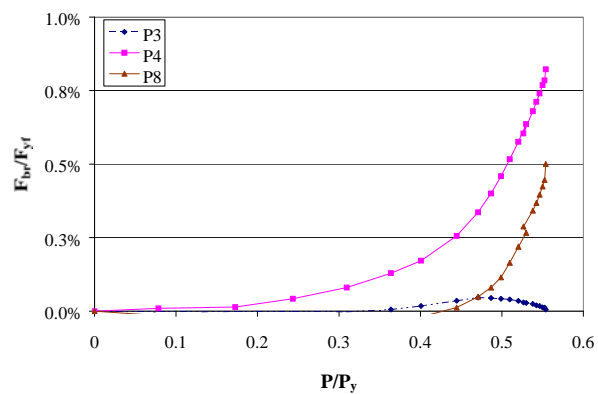
Figure 4.18 Brace Force Distribution for R10-5

4.5.2 Test R10-W

The purpose of test R10-W was to determine if the connection details used in the previous test cases had reduced the effective stiffness of the lateral bracing. This test employed the welded connection detail described in Section 3.3.2. The load-deflection response for test R10-W is shown in Figure 4.1. Lateral deflection data was, again, obtained from the same potentiometer used in the previous tests. The maximum test load achieved before failure was $0.76P_y$, an increase of 21% from the previous test case with the non-welded connection detail.
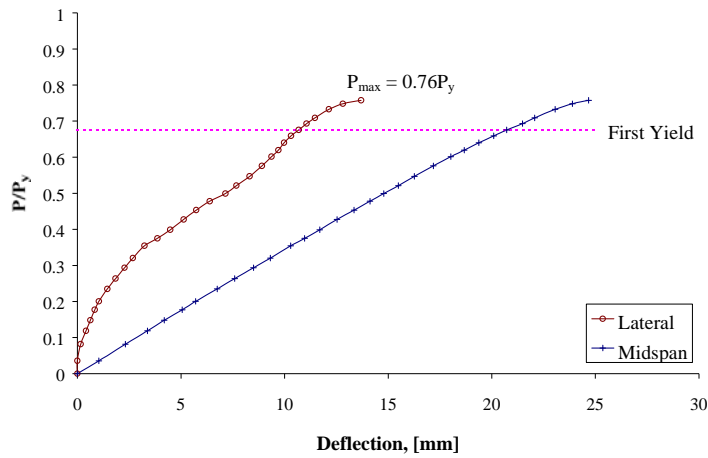
Figure 4.19 Load-Deflection Response for Test R10-W

Failure of the girder occurred by the formation of plastic hinges in the center of the third brace panel from the north support. Once these plastic hinges

64

formed, the top flanges were free to buckle, despite the presence of the diagonal bracing. That is, the flanges could buckle laterally while still maintaining the same diagonal distance between the end points of the tension brace. The locations yielding visibly observed in the whitewashed top flanges are shown in Figure 4.2 and the failure mechanism is shown in Figures 4.21 through 4.23.
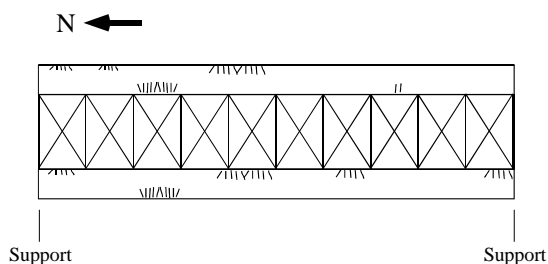
Figure 4.20 Locations of Flange Yielding
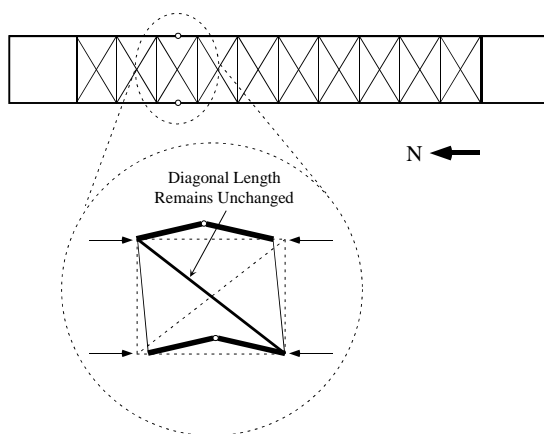
Figure 4.21 Flanges Free to Buckle Once Plastic Hinges Form

65
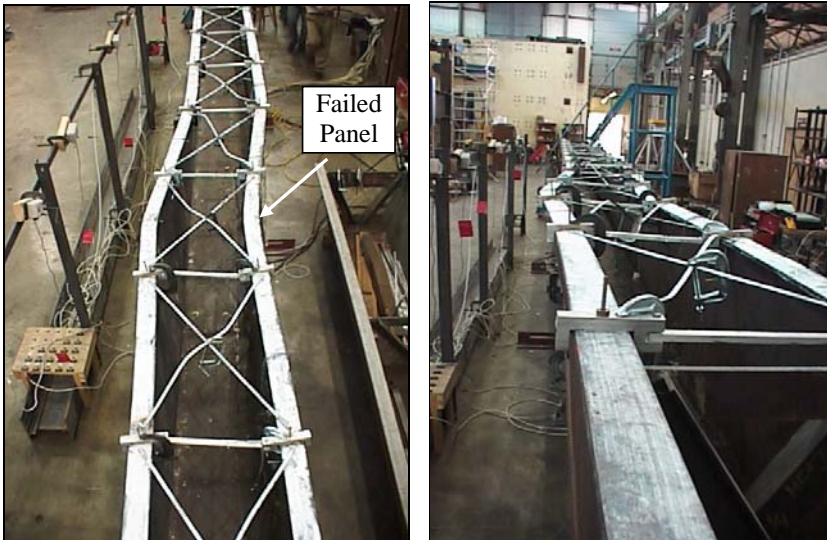
Figure 4.22 Girder After Reaching Failure Mechanism
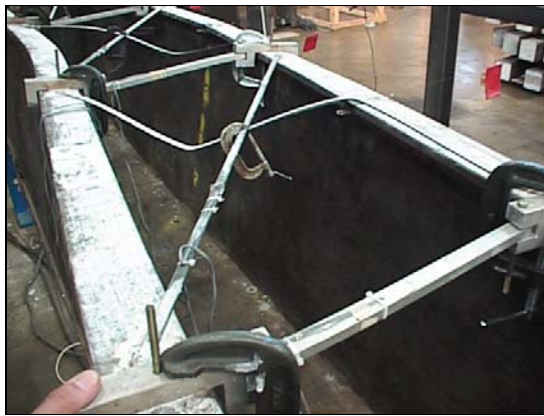
Figure 4.23 Tension Braces Still Intact After Failure

66

The out-of-plane buckled shape of the girder just before failure was the same two-wave shape seen in previous tests. However, the magnitudes of the lateral deflections were not as great for the same levels of applied load.
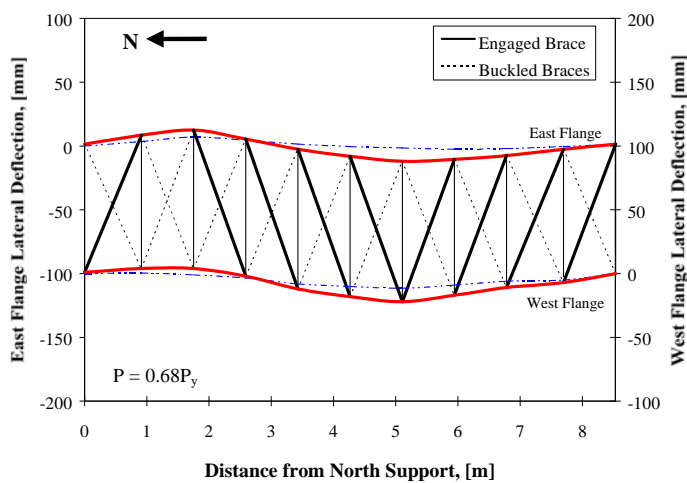
Figure 4.24 Buckled Shape for R10-W

The brace forces measured included two diagonal braces and eight cross-strut members and are shown as the heavy lines in Figure 4.7. Yielding was visibly observed in the whitewashed top flanges at an applied load of $0.68P_y$. The maximum measured diagonal brace force reached 2.33% of the flange yield force, nearly three times the maximum achieved in any of the previous tests. The cross-strut forces reached a maximum of 1.22% of the flange yield force in both tension and compression, twice the maximum any of the previous tests.

67
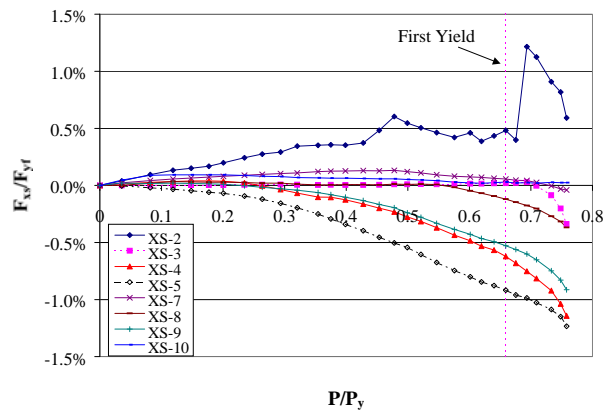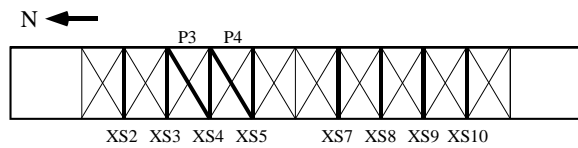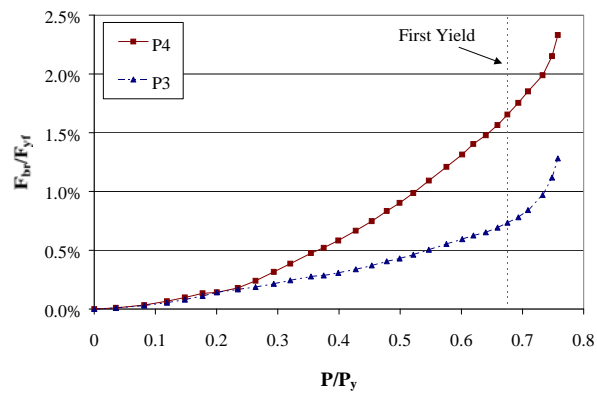
Figure 4.25 Brace Force Distribution for R10-W

4.6   BEHAVIOR OF DIAGONAL BRACES IN COMPRESSION

The diagonal braces in test R10-W were mechanically clamped together at their crossing point with c-clamps. All of the braces in compression buckled and are denoted by the dotted lines in Figure 4.6. With the exception of the two braces in the second brace panel from the north, all of the compression braces buckled into two-waves as shown in Figure 4.1. Both braces in the second brace panel were both in compression and both buckled into a single-wave.   The engaged tension braces of the other brace panels served as brace points for the compression braces, reducing their unbraced length by one half.

Figure 4.26 Diagonal Brace with Overlap Point Serving as Brace Point

CHAPTER 5

Analysis of Results

5.1 EVALUATION OF SOUTHWELL BUCKLING LOAD PREDICTIONS

Gilchrist (1997) showed that the Southwell buckling load predictions for torsionally-braced beams may not yield accurate results for buckled shapes that are more complicated than a sine wave. The Southwell predictions for the U-girder with top-flange lateral bracing were also very inconsistent. Predictions based on measurements of lateral deflection at different points along the top flange differed by significant amounts. Table 5.1 shows the typical variation in the predicted buckling loads. As with the web stiffened results presented by Gilchrist (1997), the variation in buckling loads may be caused by a buckled shape that is more complicated than a simple sine curve.

Pot #	Predicted Buckling Load (P_{cr}/P_y)	Difference from Average
1	0.60	2.3%
2	0.56	4.6%
3	0.48	17.2%
4	0.63	8.8%
5	0.58	0.1%
6	0.58	1.0%
7	0.65	11.8%
Average	0.58	--

Table 5.1 Typical Variation of Southwell Predictions Using Different Lateral Deflection Data (R5-3)

70
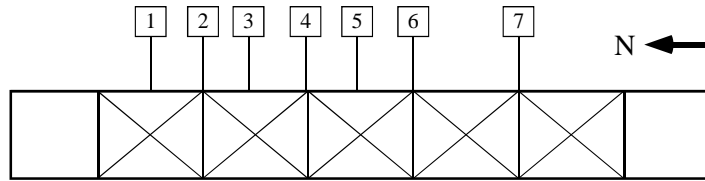
Figure 5.1 String Potentiometer Locations (R5-3)

The Southwell buckling load predictions were also very dependent on the level of load that was applied to the girder. For a given test, the Southwell predictions made using deflection data at lower applied loads differed from those made at higher load levels. This is because the Southwell method predicts buckling loads based on the assumption that elastic buckling will occur. In cases where inelastic buckling occurs, Southwell tends to overestimate the true buckling load. In these cases, the Southwell buckling loads will initially overestimate the actual buckling load, but will approach the true buckling load as the applied load approaches the true buckling load.

Figure 5.2 illustrates how the Southwell buckling load prediction decreased as the applied load increased. If only data at moderate load levels were considered, the Southwell buckling load prediction was $0.84P_y$. As the applied load increased, the slope of the data points on the Southwell plot increased, corresponding to a decrease in the predicted buckling load. The buckling load prediction when the applied load was near the true load capacity of the girder was $0.56P_y$. As the applied test load increased, the Southwell prediction converged on the true experimental buckling load of $0.55P_y$. Therefore, Southwell predictions should not be used if the buckling load, P_{cr}, exceeds the first yield load.

71
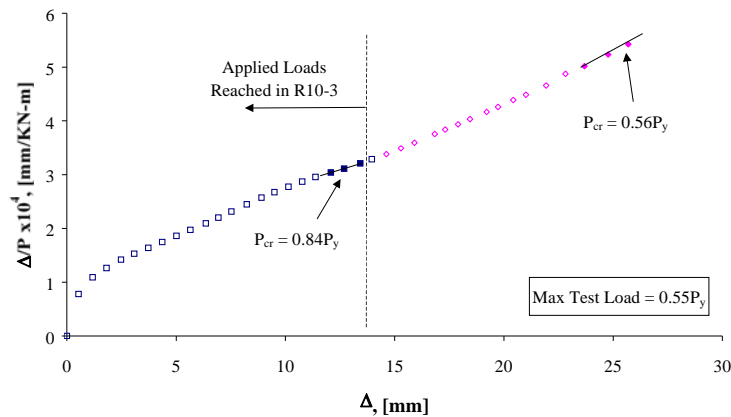
Figure 5.2 Comparison of Southwell Buckling Loads Based on Level of Applied Load (R10-4)

5.2   BRACE STIFFNESS LOSS FROM CONNECTION

The non-welded connection detail used in the experimental program did not adequately attach the diagonal bracing to the top flanges of the girder. Flexibility in the connection detail reduced the effective stiffness of the bracing system. This resulted in a significant reduction in the buckling capacity of the girder.

A comparison of tests R10-5 and R10-W isolates the effect of the brace connection detail. Test case R10-5 had the same brace geometry and even a slightly higher brace stiffness than R10-W, but the connection detail used was the removable flange mounting brackets described in Section 3.3.2. The maximum load reached during test R10-5 was $0.55P_y$, only a 17% increase from the unbraced buckling load prediction of $0.47P_y$. By contrast, the welded connection

72

in test case R10-W reached $0.76P_y$, a 62% increase over the unbraced case. Figure 5.1 compares the load versus lateral deflection responses for these two test cases. For a given load level, the lateral deflections in R10-W were much lower than in R10-5, indicating the lateral bracing was more effective at preventing lateral deflection of the top flanges. The flexibility of the non-welded connection detail decreased the effective lateral brace stiffness, thereby reducing the buckling capacity of the girder. This effect was illustrated in Section 2.3.6. Also, the lower brace stiffness of R10-5 allowed larger lateral deflections for the same load levels. The load versus midspan vertical deflection responses shown in Figure 5.2 were very similar for both test cases. Because the diagonal bracing members in test R10-W were very slender, their compressive capacity did not significantly contribute to the in-plane bending stiffness of the girder. At moderate load levels, the midspan vertical responses were nearly identical. At an applied load of about $0.35P_y$, the in-plane response of R10-5 began to deviate from linear as a result of inelasticity associated with the large lateral deflections. The deviation from linear of test R10-W occurred at an applied load of approximately $0.50P_y$. This corresponded to a significantly higher load level than test R10-5. The deviation from linear in the load versus midspan deflection response for both tests occurred at a lateral deflection of approximately 7 mm.

5.3   SHORTENING EFFECT

5.3.1   Girder Capacity Reduction

Girder bending causes shortening in the diagonal bracing such that lateral displacement must occur before the braces can return to their original length and engage. These lateral displacements, added to the initial imperfections, create second-order bending stresses in the top flanges that cause yielding to occur before P_y can be reached.

73
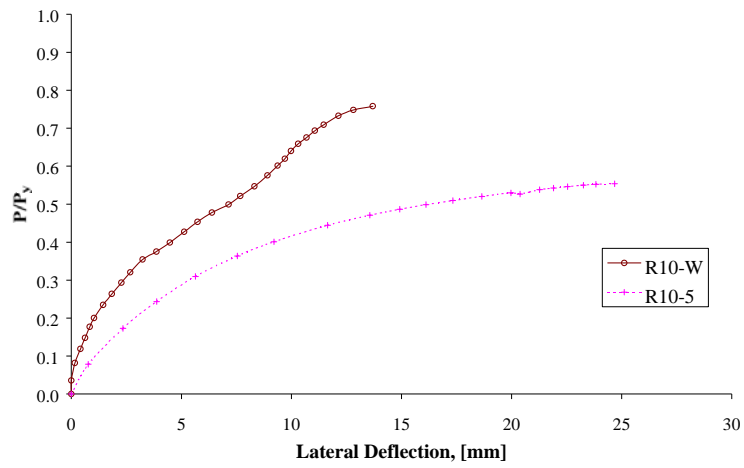
Figure 5.3 Comparison of Load vs. Lateral Deflection Responses
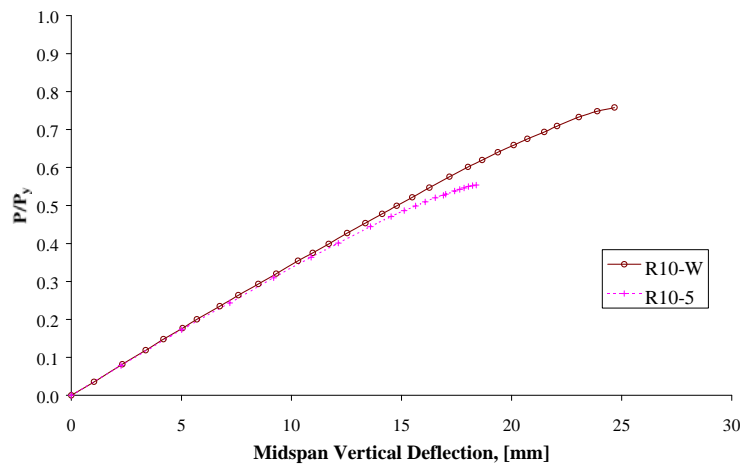
Figure 5.4 Comparison of Load vs. Midspan Vertical Deflection Responses

74

In design, the top-flange lateral bracing system is typically treated independently from the girder. In reality, however, the connection between the top flange and the bracing enforces displacement compatibility between the two. When the girder bends under loading, points along the top flange shorten due to compressive stresses. Consequently, the attached bracing also shortens, introducing slack. In order for the braces to engage, the distance between the endpoints of the diagonal braces must return to their original length. This is accommodated by lateral translation of the top flanges as illustrated in Figure 5.3.
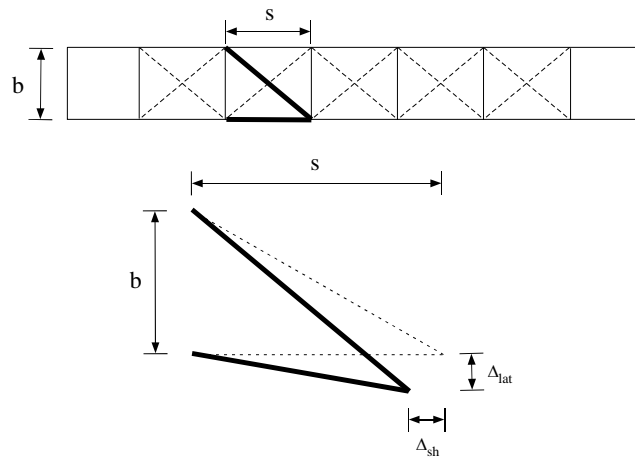
Figure 5.5 Lateral Translation of Top Flange Due to Shortening

The amount of lateral translation associated with a given amount of shortening can be obtained through simple geometry. Equating the length of a diagonal brace before and after shortening gives

$$\sqrt{s^2 + b^2} = \sqrt{(s - \Delta_{sh})^2 + (b + \Delta_{lat})^2} \tag{5.1}$$

where s is the brace panel size or brace spacing, b is the distance between the connection to the flanges, Δ_{sh} is the longitudinal shortening of the top flanges due to girder bending, and Δ_{lat} is the lateral translation necessary to accommodate the shortening. Rearranging and solving for Δ_{lat} yields

$$\Delta_{lat} = \sqrt{s^2 + b^2 - (s - \Delta_{sh})^2} - b \tag{5.2}$$

From simple bending theory, the strain multiplied by the brace panel length gives the shortening of a brace panel as

$$\Delta_{sh} = \varepsilon \cdot s = \left(\frac{M}{S_g E}\right) \cdot s \tag{5.3}$$

where M is the bending moment, S_g is the section modulus for the top of the girder, and E is Young's modulus.

The maximum compressive stress in the top flange is the sum of the first-order bending stress and second-order stress due to the lateral translation associated with shortening. The maximum lateral deflection due to shortening depends on the buckled shape of the girder. For U-shaped girders, the torsional restraint provided by the bottom flange causes the first buckling mode to be two-waves between the supports. Therefore, if the deflected shape is assumed to be a full sine wave, the maximum lateral deflection at each peak is the sum of the lateral translations of the brace panels between the support and the peak. Thus, the maximum compressive stress in the top flange equals

$$\sigma_{max} = \frac{M}{S_g} + \frac{P(n \cdot \Delta_{lat})}{S_f} \tag{5.4}$$

where P is the force in one flange, n is the number of brace panels contributing to the maximum lateral deflection, and S_f is the section modulus of a top flange about its strong axis. If the stress distribution in the top flange is approximated as uniform, then the flange force, P, is equal to

$$P = \frac{M}{S_g} A_f \qquad (5.5)$$

where A_f is the area of one top flange. To find the bending capacity of the braced girder considering the effects of shortening, the yield stress of the top flanges, F_y, is substituted for σ_{max}. Combining Equations (5.4) and (5.5) gives

$$F_y = \frac{M}{S_g}\left[1 + \frac{A_f}{S_f} n \cdot \Delta_{lat}\right] \qquad (5.6)$$

Substituting Equations (5.2) and (5.3) into (5.6) yields

$$F_y = \frac{M}{S_g}\left[1 + \frac{A_f}{S_f} n \cdot \sqrt{s^2 + b^2 - \left(s - \frac{M \cdot s}{S_g E}\right)^2} - \frac{A_f}{S_f} b\right] \qquad (5.7)$$

Solving for M gives the bending capacity of a girder considering the effects of elastic shortening.

5.3.2 Comparison of Theoretical Capacity and Results from R10-W

The "Full Bracing" criteria developed by Winter was defined as forcing buckling between brace points and considering the brace points themselves to be unyielding supports. For a girder with no initial imperfections and unyielding brace points, the load capacity would either be governed by buckling between brace points or flange yielding. In the case of test R10-W, buckling between brace points corresponded to a load above the yield load, P_y. Analysis using

77

Winter's "Full Bracing" criteria would predict a load capacity equal to P_y, but the experimental test reached a maximum applied load of only $0.76P_y$.

An analysis was conducted to determine the capacity of the girder with ten brace panels, considering the effects of shortening as described in the previous section. The yield stress used was the average static yield stress of the top flanges obtained from the tensile tests, F_{sy}, and was equal to 320 MPa (46.4 ksi).

The maximum moment was obtained by numerically solving for the moment, M, in Equation (5.7). Since the buckled shape was two-waves between the supports, one-quarter of the brace panels were estimated to contribute to the maximum lateral deflection. The value of n was estimated to be equal to 2.5, the total number of brace panels between supports, ten, divided by four. Although the value of n was not an integer and the true peaks were not located at the quarter points, the calculation provides a reasonable approximation of the maximum lateral deflection due to girder shortening. The results of this analysis indicated that the top flanges of the girder would yield at an applied load of $0.72P_y$. Thus, the effects of shortening alone can reduce the bending capacity of a U-shaped girder by a significant amount.

A comparison of the girder's strength with varying brace angles is shown in Figure 5.1. The curve plotted represents the load at which first yield would occur in the top flanges due to the combined first and second-order stresses. Increasing the brace angle, θ, decreases the girder's capacity non-linearly because the lateral deflections due to shortening increase with increasing brace angles.

The previous analysis was not intended to reproduce the experimental load capacity analytically, but to illustrate the detrimental effects of shortening. Some additional factors which were not considered in the analysis include lateral deflections due to initial imperfections of the top flanges or elongation of the

brace members, additional compressive stresses induced in the top flanges by tension brace forces, strain hardening, and residual stresses.
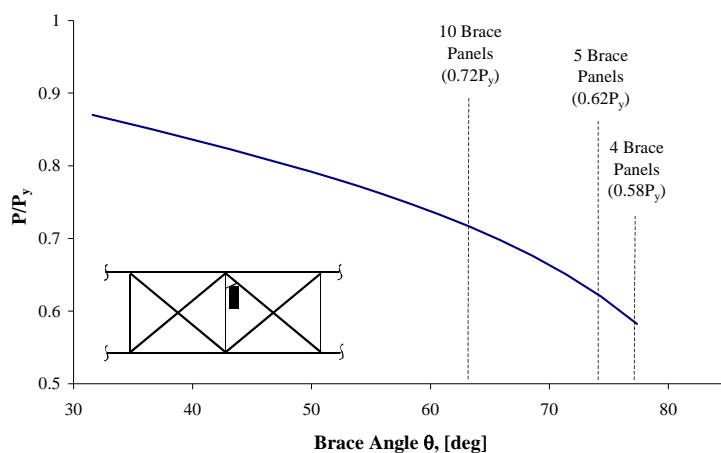
Figure 5.6 Effect of Shortening on Girder Capacity

The nominal flexural resistance of the U-girder was also calculated using the current *AASHTO LRFD Bridge Design Specifications*. Similar results would have been obtained using the *AISC LRFD Specification for Steel Buildings*. Using the unbraced length of the ten brace panel geometry and the average static yield stress, F_{sy}, the nominal flexural strength calculated was $0.95P_y$. Details of the calculations may be found in Appendix B1. By comparison, the flexural strength of the girder considering the effects of shortening was $0.72P_y$. This discrepancy can be attributed to the fact that the current specifications do not account for the effects of shortening.

79

5.4 BRACE FORCES

Current design recommendations for beam lateral bracing follow from the column analogy presented in Section 2.3.1. The value of the brace force at arbitrary applied loads is given by

$$F_{brace} = \frac{M/h}{\cos\theta}\left(\frac{\Delta_o}{s}\right)\left(\frac{1}{1 - \dfrac{M/h}{s\beta}}\right) \tag{5.8}$$

where M is the girder moment, h is the height of the girder, Δ_o/s is the initial out-of-straightness of the brace panel, and β is the effective lateral brace stiffness (Yura, 1993, also refer to Figure 2.1 and Appendix B2). The ratio M/h represents an equivalent compressive beam flange force and is applicable for both the elastic and inelastic regions. Predicted values were obtained both considering and not considering the effects of shortening. Shortening increases the brace forces by effectively increasing the out-of-straightness of a brace panel. The initial out-of-straightness term Δ_o is replaced by $\Delta_o + \Delta_{sh}$. Brace geometries with larger brace angles (fewer brace panels) exhibit larger brace force increases because Δ_{sh} is greater for larger brace angles.

A comparison between the brace forces calculated using Equation (5.8) and the experimentally measured values obtained in test R10-W is shown in Figure 5.1. The average initial out-of-straightness values of 0.003 and 0.0045 for were used for brace panels three and four, respectively (see Table A.5). Brace force predictions when the effects of shortening were not considered compared favorably with the measured results for P3 but underestimated P4. When shortening was considered, calculated values agreed well with measured results for P4 but overestimated P3. Differences between calculated and measured results stem from both the sensitivity to the value chosen for the initial out-of-

80

straightness, as well as the theoretical predicted deflections due to shortening. Results obtained using Equation (5.8), however, follow the general trend exhibited by the measured brace forces.
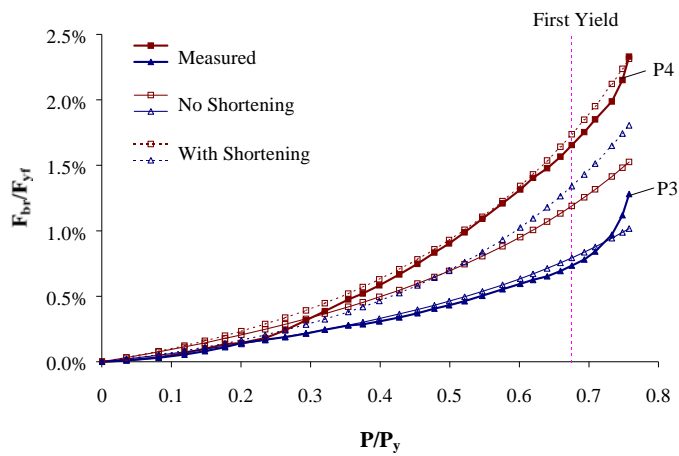
Figure 5.7 Comparison of Measured and Calculated Brace Forces (R10-W)

Cross-strut forces can be determined from the value of the diagonal brace forces and the brace geometry. By applying static equilibrium to a brace connection joint, the cross-strut force becomes equal to the lateral components of the diagonal brace forces. A comparison of the measured and calculated cross-strut forces for the fourth brace panel in R10-W is shown in Figure 5.2. The small compressive force due to the compression diagonal buckling was ignored. The calculated cross-strut force compares favorably with the average of the two

81

measured forces. The difference between the two strut forces was due to the lateral bending stiffness of the flanges.
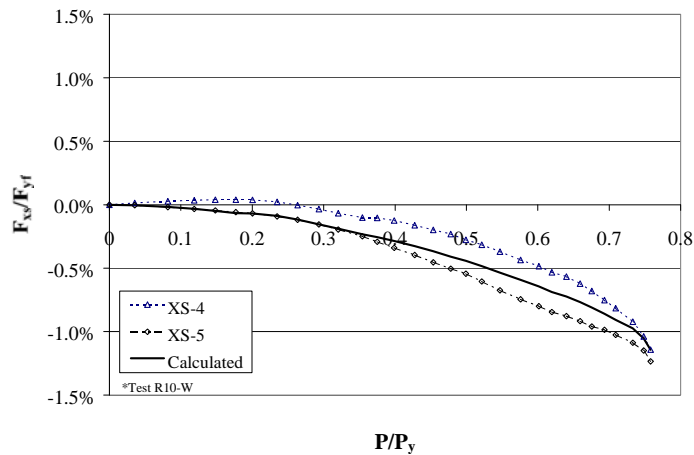
Figure 5.8 Comparison of Calculated and Measured Cross-Strut Forces

5.5 COMPARISON OF BUCKLED SHAPES

The buckled shape of the girder for all the test cases was two-waves between the supports. A comparison of the buckled shapes for the various test cases at similar load levels is shown in Figure 5.1. Despite variations in the brace spacing or stiffness, the eventual buckled shape of the girder remained the same.

The diagonal bracing was unable to force a higher buckling mode partly because of the effects of shortening. Even for an infinitely stiff tension-only brace, shortening would accommodate some lateral deflection of the top flanges. As a result, the girder would be able to deflect into its preferred buckled shape. In

82

this case, the torsional restraint of the bottom flange made the preferred shape two-waves.
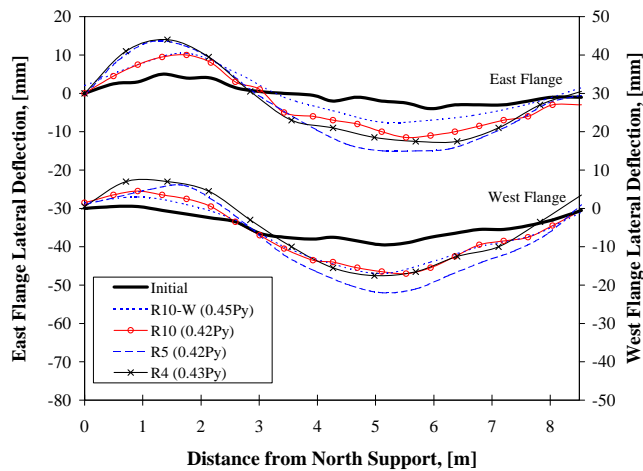
Figure 5.9 Comparison of Deflected Shapes for Different Brace Geometries

5.6   TENSION-ONLY VS. TENSION-COMPRESSION BRACING SYSTEMS

Unlike tension-only bracing systems, tension-compression systems (X-brace) increase the bending stiffness of the girder by attracting a portion of the flange stresses. The bending behavior of a girder with a tension-compression top-flange lateral bracing system can be analyzed by effectively increasing the area of the top flanges (Fan, 1999).

Girder shortening affects both tension-only and tension-compression systems alike. The difference between the two systems is tension-compression systems have a nominal compressive resistance. As the panel attempts to distort, the compression brace can help prevent such movement. However, since the

83

buckling capacity of the diagonal braces is typically very low, design neglects the stiffness provided by the braces in compression. For X-brace systems, only two braces, one in each of the adjacent brace panels, and not four are considered to contribute to the lateral brace stiffness at a particular brace point.

The advantage of the tension-compression system is the increase in girder stiffness that the bracing provides. By attracting some of the girder bending stresses, the bracing reduces the flange stresses. This in turn increases the load at which the flanges will buckle and decreases the effects of shortening. The drawback of a tension-compression system is the diagonal braces attract large axial and bending forces (Fan, 1999). Therefore, the connection detailing must have adequate ductility to accommodate brace buckling.

CHAPTER 6

Summary and Conclusions

6.1   SUMMARY

Steel box girder systems are being used more frequently for curved bridges because of their torsional stiffness and aesthetic appearance. These systems typically consist of U-shaped girders placed side-by-side with a composite concrete deck acting as the top flange. A critical design stage for these girders occurs during casting of the bridge deck, when the non-composite steel section must support the entire construction load, including the wet concrete. During this period the top flanges are in compression and are susceptible to lateral-torsional buckling. Lateral bracing, typically in the form of a horizontal truss system, is installed to prevent the flanges from buckling and to increase the torsional stiffness of the girders. There is currently no existing codified design method for the lateral bracing of U-shaped girders. Because the bracing is not utilized once the concrete deck has cured, minimizing the amount of bracing will lead to more efficient designs.

In order to develop a design procedure, it was first necessary to understand the effect of the top-flange lateral bracing on the bending strength of U-shaped girders. An analytical study was conducted using elastic finite element modeling. Bifurcation loads and buckling modes obtained in the analysis were used to guide the selection of appropriate experimental test cases. Experimental tests were then conducted on a scale model of a rectangular U-shaped girder. Variable parameters included brace stiffness, geometry, initial pretension force, and connection detail. The scope of the investigation was limited to tension-only top-flange lateral bracing systems. Experimental test results provided girder buckling

85

loads and buckled shapes to compare with the analytical results. Brace forces, which could not be obtained in the analytical program, were measured to compare with current design provisions.

6.2   CONCLUSIONS FROM ANALYTICAL PROGRAM

Conclusions from this analytical study indicated that:

1. Top-flange lateral bracing can significantly increase the buckling capacity of a U-girder. Increasing the brace stiffness results in a non-linear increase in the buckling capacity and a switch to higher buckling modes. Increasing the number of brace panels also increases the buckling capacity.

2. Top-flange torsional or rotational restraint at the locations of brace points does not affect the buckling behavior of a U-girder at moderate stiffness levels. Full torsional restraint of the top flanges can increase the buckling capacity significantly.

6.3   CONCLUSIONS FROM EXPERIMENTAL PROGRAM

Current design provisions for U-shaped girders consider brace points as unyielding supports. The bending strength, which is normally controlled by lateral torsional buckling, is based upon the unbraced length of the top compression flanges. Girder bending, however, can affect the behavior of the top-flange lateral truss system used to brace the girder. This can result in a significant reduction in the girder's bending capacity and increase in brace forces.

Girder bending causes the brace panels of a U-girder with a top-flange lateral truss system to shorten. Consequently, slack is introduced into the diagonal bracing. Lateral displacement of the top flanges must then occur before the braces can return to their original length and engage. This lateral displacement increases the second-order bending stresses in the top flanges,

which reduce the girder's bending capacity. Current design provisions do not account for the effects of shortening. For the test case with the welded connection detail, the experimental load capacity was 20% less than the nominal flexural resistance calculated using current specifications.

The increased lateral deflections of the top flange due to shortening also increase the brace forces by effectively increasing the out-of-straightness of the brace panels. For the test case with the welded connection detail, brace force increases ranged from 50-75%, depending on the initial out-of-straightness of the brace panels. Again, current design specifications do not account for the brace force increases associated with shortening.

Other conclusions from the experimental program were:

1. The Southwell predicted buckling loads might not be reliable when the buckled shape is more complicated than a sine wave. The deformed shape of the test girder may have deviated from the sine wave because of the presence of the top-flange lateral bracing.

2. The Southwell predicted buckling loads overestimated the true buckling load when inelastic buckling occurred. The Southwell loads approached the experimental buckling load as the applied load approached the buckling load.

3. The removable connection detail between the diagonal braces and the top flange significantly decreased the effective stiffness of the braces. As a result, the buckling capacity of the girder was significantly reduced.

4. The ultimate load capacities obtained from the experimental tests were less than those predicted by the Southwell Method and elastic finite element analyses (BASP). Because discrete braces were used in the analytical model to approximate relative braces, the effects of shortening were not accounted for.

87

5. The tension diagonal braces acted as brace points for compression diagonal braces, reducing their unbraced length by one-half.
6. The buckled shape for all unbraced and braced test cases was two-waves between the supports.

6.4 FUTURE RESEARCH

The results of the experimental program showed the increase in buckling capacity that a lateral bracing system could provide. Because of the problems associated with the removable connection detail, only one welded brace stiffness/geometry case was conducted. Additional tests may be necessary to verify that the effect of changing brace stiffness and geometry can be adequately predicted using the current analytical models. Large displacement analyses may also be necessary to better understand the brace forces that are developed in relative bracing systems.

In addition to providing stability to the top flanges during bending, top lateral brace systems effectively close the section and increase the torsional rigidity of a U-girder. Brace forces due to torsion in these curved girders have been predicted analytically and measured in the field (Fan, 1999), but experimental data is currently limited to only single-diagonal bracing systems.

The use of the corrugated metal decking has been proposed for use as the lateral bracing for the top flanges of a U-girder. The advantage of the metal decking is that it is not susceptible to the effects of shortening that diagonal bracing systems are. Metal decks oriented with their ribs perpendicular to the length of a beam have the ability to shorten as the girder bends without introduce slack into the bracing system. That is, even after the flanges have shortened, the metal decks are able to immediately engage to prevent any lateral deflection.

88

Currently, however, there has been no experimental research conducted to verify the effectiveness of the metal decking as a lateral bracing system.

APPENDIX A

A.1 TENSILE TEST DATA

	F_{uy} MPa (ksi)	F_{sy} MPa (ksi)	F_{uu} MPa (ksi)	F_{su} MPa (ksi)	% Elongation
Top Flange	342.2 (49.6)	323.2 (46.9)	467.9 (67.9)	-	-
	341.9 (49.6)	313.9 (45.5)	469.0 (68.0)	444.1 (64.4)	37.8%
	345.4 (50.1)	321.5 (46.6)	464.6 (67.4)	441.6 (64.0)	39.3%
	343.2 (49.8)	321.9 (46.7)	470.0 (68.2)	442.7 (64.2)	37.3%
	Average	**320.1 (46.4)**		**442.8 (64.2)**	
Web	322.1 (46.7)	300.6 (43.6)	425.5 (61.7)	401.1 (58.2)	27.9%
	324.5 (47.1)	299.7 (43.5)	492.5 (71.4)	443.4 (64.3)	28.9%
	Average	**300.2 (43.5)**		**422.3 (61.2)**	
Bottom Flange	328.9 (47.7)	309.3 (44.9)	468.2 (67.9)	440.5 (63.9)	25.4%
	337.1 (48.9)	320.2 (46.4)	475.9 (69.0)	446.8 (64.8)	27.3%
	Average	**314.8 (45.7)**		**443.6 (64.3)**	

F_{uy} – Upper Yield Stress
F_{sy} – Static Yield Stress (5 minutes)
F_{uu} – Upper Ultimate Stress
F_{su} – Static Ultimate Stress (5 Minutes)

Table A.1 Tensile Test Data

A.2 COUPLER CALIBRATION FACTORS

Coupler #	Calibration Factor [KN/$\mu\varepsilon$]
1	0.0143
2	0.0153
3	0.0152
4	0.0149
5	0.0164
6	0.0168
7	0.0164
8	0.0157
9	0.0131
10	0.0149
11	0.0155
12	0.0182

Table A.2 Coupler Calibration Factors

A.3 OUT-OF-STRAIGHTNESS VALUES

Brace Panel (from North)	Panel Size	East		West	
		Δ_o	Δ_o/s	Δ_o	Δ_o/s
	[mm]	[mm]		[mm]	
1	2134	4.3	0.0020	3.5	0.0016
2	2134	4.1	0.0019	5.0	0.0023
3	2134	3.3	0.0015	2.0	0.0009
4	2134	3.1	0.0015	6.5	0.0030
		Max =			**0.0030**

Table A.3 Out-of-Straightness Values for 4 Brace Panel Tests

Brace Panel (from North)	Panel Size	East		West	
		Δ_o	Δ_o/s	Δ_o	Δ_o/s
	[mm]	[mm]		[mm]	
1	1707	6.5	0.0038	3.5	0.0021
2	1707	5.5	0.0032	5.0	0.0029
3	1707	2.5	0.0015	1.0	0.0006
4	1707	0.5	0.0003	3.0	0.0018
5	1707	2.0	0.0012	6.0	0.0035
		Max =	**0.0038**		

Table A.4 Out-of-Straightness Values for 5 Brace Panel Tests

Brace Panel (from North)	Panel Size	East		West	
		Δ_o	Δ_o/s	Δ_o	Δ_o/s
	[mm]	[mm]		[mm]	
1	838	3.5	0.0042	0.5	0.0006
2	838	3.5	0.0042	1.5	0.0018
3	838	2.5	0.0030	2.5	0.0030
4	838	3.0	0.0036	4.5	0.0054
5	838	2.0	0.0024	2.0	0.0024
6	838	1.0	0.0012	1.5	0.0018
7	838	1.0	0.0012	2.5	0.0030
8	838	0.5	0.0006	3.0	0.0036
9	838	1.5	0.0018	1.0	0.0012
10	838	2.0	0.0024	5.0	0.0060
		Max =			**0.0060**

Table A.5 Out-of-Straightness Values for 10 Brace Panel Tests
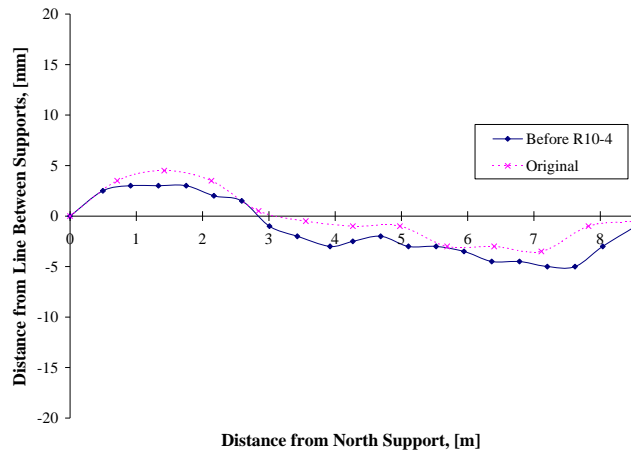
A.4 TEST R4-4
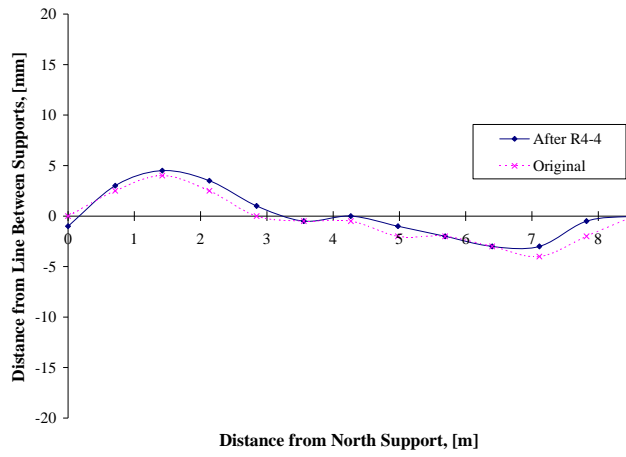
Figure A.1 Permanent Set of East Flange After Test R4-4
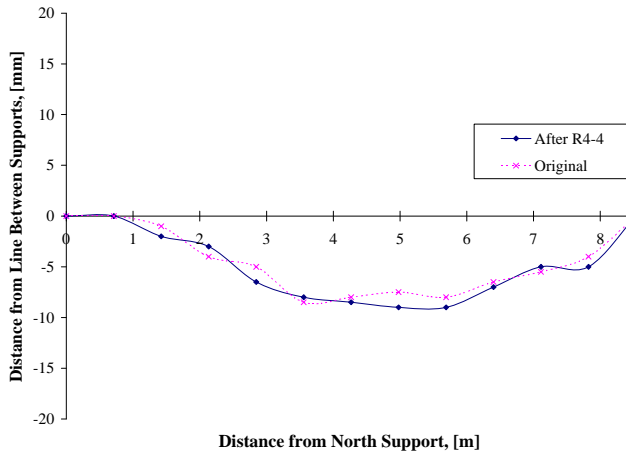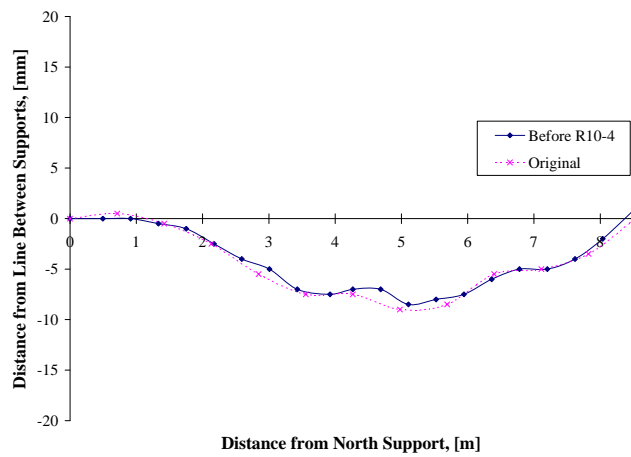

Figure A.2 Permanent Set of West Flange After Test R4-4

94

A.5 TEST R10-4

Figure A.3 Initial Imperfections of East Flange Before Test R10-4

Figure A.4 Initial Imperfections of West Flange Before Test R10-4

95

Figure A.5 Load-Deflection Response for Test R10-4

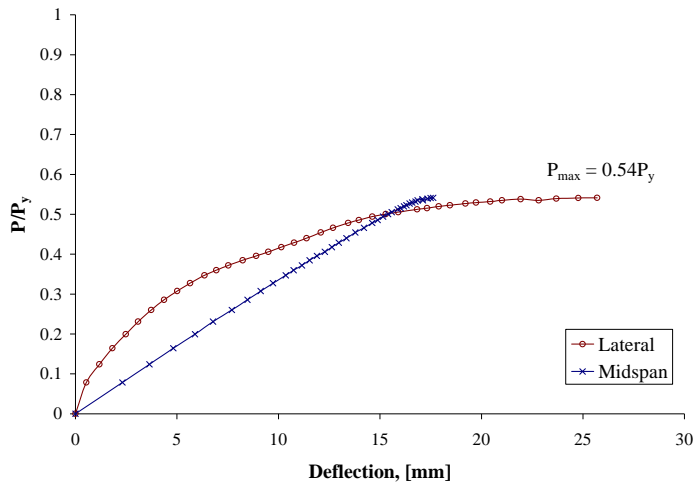*Figure A.6 Brace Force Distribution for Test R10-4*

97

A.6   TEST R10-5

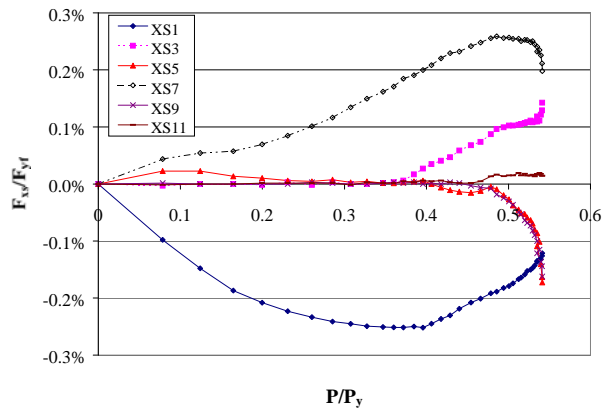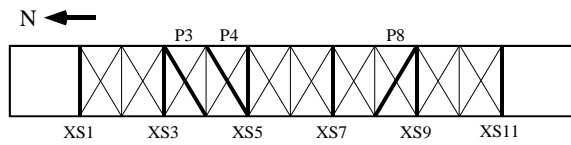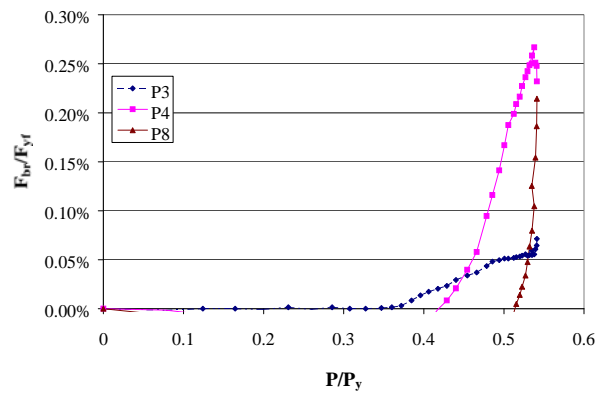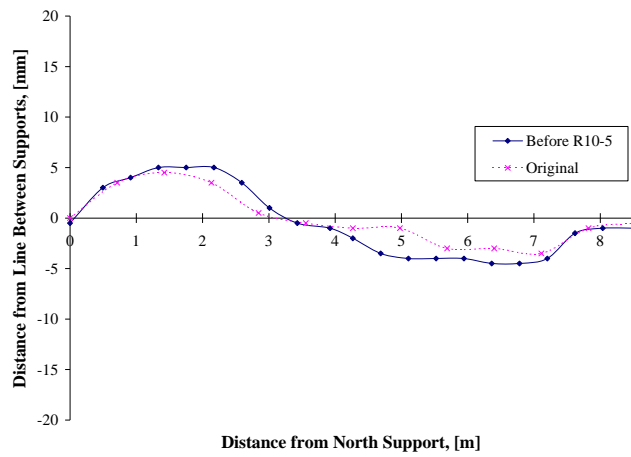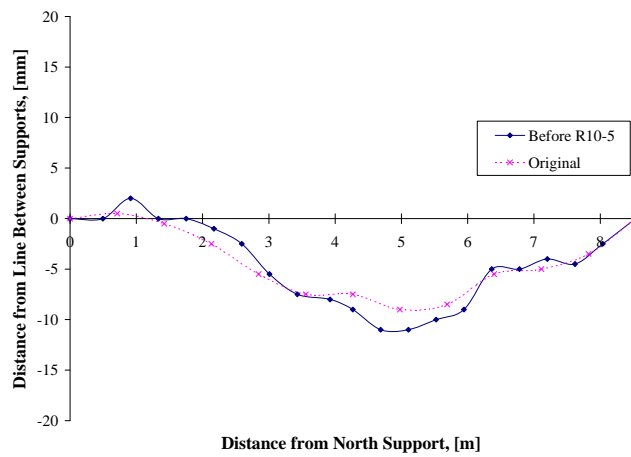**Figure A.7 Initial Imperfections of East Flange Before Test R10-5**

Figure A.8 Initial Imperfections of West Flange Before Test R10-5

98

APPENDIX B

B.1 CALCULATIONS FOR DESIGN FLEXURAL STRENGTH OF U-GIRDER

The flexural resistance of the U-girder used in the experimental program with top-flange lateral bracing was calculated using the *1998 AASTHO LRFD Bridge Design Specifications*. The equations used for lateral torsional buckling of noncompact sections are the same as those in the *AISC LRFD Specification for Steel Buildings*.

6.10.4.1.9 Noncompact Section Compression-Flange Bracing

$$E = 29000 \, \text{ksi}$$

$$F_{yc} = \text{Avg. Experimental Static Yield Stress} = 46.4 \, \text{ksi (see Appendix A1)}$$

$$I_t = \frac{1}{12}(0.505)(3.056)^3 + \frac{1}{12}\left(\frac{24.813}{3}\right)(0.253)^3 = 1.21 \, \text{in}^4$$

$$A_t = (0.505)(3.056) + \left(\frac{24.813}{3}\right)(0.253) = 3.64 \, \text{in}^2$$

$$r_t = \sqrt{\frac{I_t}{A_t}} = \sqrt{\frac{1.21}{3.64}} = 0.58 \, \text{in.}$$

$$L_p = 1.76 \cdot r_t \sqrt{\frac{E}{F_{yc}}} = 1.76 \cdot (0.58)\sqrt{\frac{29000}{46.4}} = 25.4 \, \text{in}$$

Since all $L_b > L_p$ for all brace geometries considered, use 6.10.4.2.6

6.10.4.2.6 Noncompact Section Flexural Resistance Based Upon Lateral Torsional Buckling

$$D_c = \frac{I_x}{S_x} - t_f = \frac{2676}{155.0} - 0.505 = 16.8 \text{ in.}$$

$$\left[\frac{2D_c}{t_w} = \frac{2(16.8)}{0.253} = 132.5 \right] > \left[\lambda_b \sqrt{\frac{E}{F_{yc}}} = 4.64 \sqrt{\frac{29000}{46.4}} = 116 \right]$$

where $\lambda_b = 4.64$ for members with compression - flange area

less than tension flange area

Calculate L_r

$$I_{yc} = \frac{1}{12} t_f b_f^3 = \frac{1}{12}(0.505)(3.056)^3 = 1.20 \text{ in}^4$$

$$S_{xc} = \frac{I_{yc}}{t_f/2} = \frac{1.20}{0.505/2} = 4.76 \text{ in}^3$$

$$d = 0.505 + 24.813 + 0.640 = 26.0 \text{ in}$$

$$L_r = 4.44 \sqrt{\frac{I_{yc}d}{S_{xc}} \frac{E}{F_{yc}}} = 4.44 \sqrt{\frac{(1.20)(25.96)}{(4.75)} \frac{(29000)}{(46.4)}} = 284 \text{ in.}$$

since all L_b are $< L_r$, use Eqn. (6.10.4.2.6a - 2)

Calculate Moment Capacity

since $\frac{2D_c}{t_w} > \lambda_b \sqrt{\frac{E}{F_{yc}}}$

$$a_r = \frac{2D_c t_w}{A_c} = \frac{2(16.8)(0.253)}{1.54} = 5.5$$

$$R_b = 1 - \left(\frac{a_r}{1200 + 300 a_r} \right) \left(\frac{2D_c}{t_w} - \lambda_b \sqrt{\frac{E}{F_c}} \right)$$

$$= 1 - \left(\frac{5.5}{1200 + (300)(5.5)} \right) \left(\frac{2(16.8)}{0.253} - 4.64 \sqrt{\frac{29000}{46.4}} \right)$$

$$= 0.97$$

$$M_n = C_b R_b R_h M_y \left[1 - 0.5 \left(\frac{L_b - L_p}{L_r - L_p} \right) \right]$$

$$= (1.0)(0.97)(1.0) M_y \left[1 - 0.5 \left(\frac{33.0 - 25.4}{284 - 25.4} \right) \right]$$

$$= 0.95 M_y$$

Summary of results for the various test cases are listed below. Nominal flexural resistance values are reported in terms of P_n/P_y because of the direct relationship between the ram load and girder moment in the experimental test setup.

# Brace Panels	Unbraced Length, L_b [in.]	$\dfrac{P_n}{P_y}$
10	33.0	0.95
5	66.0	0.89
4	82.5	0.86

Table B.1 Nominal Flexural Strength of Girder Using Current Design Specifications

B.2 DERIVATION OF BRACE FORCE EQUATION (5.8)

Referring to Figure 2.1

$$\Delta_T = \Delta_o + \Delta$$

$$P\Delta_T = F_{br}L$$

$$\frac{P}{L}\Delta_T = \beta(\Delta_T - \Delta_o)$$

$$\beta\Delta_o = \Delta_T\left(\beta - \frac{P}{L}\right)$$

$$\Delta_T = \Delta_o \frac{\beta}{\beta - P/L}$$

$$\Delta_T = \Delta_o \frac{1}{1 - P/\beta L}$$

Now calculating for the brace force using cosine function to convert to a diagonal brace gives:

$$F_{br} = (\Delta_T - \Delta_o)\frac{\beta}{\cos\theta}$$

$$= \left(\frac{1}{1 - P/\beta L} - 1\right)\frac{\beta\Delta_o}{\cos\theta}$$

$$= \left(\frac{P/\beta L}{1 - P/\beta L}\right)\frac{\beta\Delta_o}{\cos\theta}$$

$$= \frac{P}{\cos\theta}\left(\frac{\Delta_o}{L}\right)\left(\frac{1}{1 - P/\beta L}\right)$$

$$\therefore F_{br} = \frac{P}{\cos\theta}\left(\frac{\Delta_o}{L}\right)\left(\frac{1}{1 - P/\beta L}\right)$$

In terms of calculations for the braced U-girder, replace P with M/h and L with the brace panel length, s.

$$F_{brace} = \frac{M/h}{\cos\theta}\left(\frac{\Delta_o}{s}\right)\left(\frac{1}{1 - \dfrac{M/h}{s\beta}}\right)$$

103

REFERENCES

AASHTO LRFD Bridge Design Specifications, American Association of State Highway and Transportation Officials, 1996.

Akay, H. U., Johnson, C. P., and Will, K. M. (1977). "Lateral and Local Buckling of Beams and Frames." *Journal of the Structural Division*, Vol. 103(9), ASCE, New York, N.Y., pp. 1821-1832.

Basler, K. and Kollbrunner, C. F. (1969). *Torsion in Structures.* Springer-Verlag, Berlin, Germany, pp. 14-15.

Bažant, Z. P. and Cedolin, L. (1991). *Stability of Structures.* Oxford University Press, Inc., New York, N.Y., pp. 19-26.

Choo, K. M., (1987). "Buckling Program BASP for Use on a Microcomputer," thesis presented to The University of Texas at Austin, in partial fulfillment of the requirements for the degree of Doctor of Philosophy.

Fan, Zhanfei. (1999). "Field and Computational Studies of Steel Trapezoidal Box Girder Bridges," thesis presented to The University of Houston, in partial fulfillment of the requirements for the degree of Doctor of Philosophy.

Gilcrhist, Christopher. (1997). "Buckling Behavior of U-Shaped Girders," thesis presented to The University of Texas at Austin, in partial fulfillment of the requirements for the degree of Master of Science in Engineering.

Guide Specifications for Horizontally Curved Highway Bridges, American Association of State Highway and Transportation Officials, 1993.

Load and Resistance Factor Design Specification for Steel Buildings, American Institute of Steel Construction, December, 1993.

Meck, H. R. (1977). "Experimental Evaluation of Lateral Buckling Loads." *Journal of the Engineering Mechanics Division*, ASCE, EM2, April, pp. 331-337.

Southwell, R. V. (1932). "On the Analysis of Experimental Observations in the Problems of Elastic Stability.*" Proceedings of the Royal Philosophical Society of London*, Series A, Vol. 135, April, p. 601.

Taylor, A. C., and Ojalvo, M. (1966). "Torsional Restraint of Lateral Buckling." *Journal of the Structural Division*, Vol. 92(ST2), ASCE, New York, N.Y., pp. 115-129.

Timoshenko, S., and Gere, J. (1961). *Theory of Elastic Stability.* McGraw-Hill Book Company, New York, N.Y., pp. 190-191.

Trahair, Nicholas S. (1969). "Deformations of Geometrically Imperfect Beams." *Journal of the Structural Division*, Vol. 95(7), ASCE, New York, N.Y., pp. 1475-1496.

Winter, G. (1960). "Lateral Bracing of Columns and Beams." *ASCE Transactions*, Vol. 125, ASCE, New York, N.Y., pp. 809-825.

Yura, Joseph A. (1993). "Fundamentals of Beam Bracing." Structural Stability Research Council Conference - Is Your Structure Suitably Braced?, April 6-7, Milwaukee, WI.

Yura, Joseph A. (1995). "Bracing for Stability-State-of-the-Art" Proceedings, Structures Congress XIII, ASCE, Boston, MA, April, pp. 88-103.

Yura, Joseph A. (1996). "Winter's Bracing Approach Revisited." *Engineering Structures*, Vol. 18(10), Elsevier Science Ltd., Great Britain, pp. 821-825.

VITA

Brian Scott Chen was born in Bethlehem, Pennsylvania to Wai-Fah and Lily Chen in October of 1975. After graduating from West Lafayette High School in June of 1993, he entered Purdue University that same fall. In May of 1997, he received his bachelor of science degree in civil engineering with highest distinction.

In August of 1997, he enrolled in the graduate program in civil engineering at The University of Texas at Austin. He has been employed as a graduate research assistant while pursuing his master of science degree. He plans to continue at The University of Texas at Austin in pursuit of his doctorate.

Permanent address: 501 W. 26th St. #121
                       Austin, TX 78705

This thesis was typed by the author.